

## Journal Pre-proof

Tropical peat subsidence rates are related to decadal LULC changes: Insights from InSAR analysis

Deha Agus Umarhadi, Wirastuti Widyatmanti, Pankaj Kumar, Ali P. Yunus, Khaled Mohamed Khedher, Ali Kharrazi, Ram Avtar



PII: S0048-9697(21)06639-0

DOI: <https://doi.org/10.1016/j.scitotenv.2021.151561>

Reference: STOTEN 151561

To appear in: *Science of the Total Environment*

Received date: 2 July 2021

Revised date: 5 October 2021

Accepted date: 5 November 2021

Please cite this article as: D.A. Umarhadi, W. Widyatmanti, P. Kumar, et al., Tropical peat subsidence rates are related to decadal LULC changes: Insights from InSAR analysis, *Science of the Total Environment* (2021), <https://doi.org/10.1016/j.scitotenv.2021.151561>

This is a PDF file of an article that has undergone enhancements after acceptance, such as the addition of a cover page and metadata, and formatting for readability, but it is not yet the definitive version of record. This version will undergo additional copyediting, typesetting and review before it is published in its final form, but we are providing this version to give early visibility of the article. Please note that, during the production process, errors may be discovered which could affect the content, and all legal disclaimers that apply to the journal pertain.

© 2021 Published by Elsevier B.V.

**Tropical peat subsidence rates are related to decadal LULC changes: Insights from InSAR analysis**

Deha Agus Umarhadi<sup>1</sup>, Wirastuti Widyatmanti<sup>2</sup>, Pankaj Kumar<sup>3</sup>, Ali P. Yunus<sup>4,5</sup>, Khaled Mohamed Khedher<sup>6,7</sup>, Ali Kharrazi<sup>8,9</sup>, Ram Avtar<sup>1,10\*</sup>

<sup>1</sup>Graduate School of Environmental Science, Faculty of Environmental Earth Science, Hokkaido University, Sapporo, Japan

<sup>2</sup>Department of Geographic Information Science, Faculty of Geography, Universitas Gadjah Mada, Yogyakarta, Indonesia

<sup>3</sup>Natural Resources and Ecosystem Services, Institute for Global Environmental Strategies, Hayama, Japan

<sup>4</sup>State Key Laboratory of Geohazard Prevention and Geoenvironment Protection, Chengdu University of Technology, Chengdu, China

<sup>5</sup>Center for Climate Change Adaptation, National Institute for Environmental Studies, Tsukuba, Japan

<sup>6</sup>Department of Civil Engineering, College of Engineering, King Khalid University, Abha 61421, Saudi Arabia

<sup>7</sup>Department of Civil Engineering, High Institute of Technological Studies, Mrezgua University Campus, Nabeul 8000, Tunisia

<sup>8</sup>Advanced Systems Analysis Group, International Institute for Applied Systems Analysis, Schlossplatz 1, A-2361 Laxenburg, Austria

<sup>9</sup>Faculty of International Liberal Arts Global Studies Program, Akita International University,  
Okutsubakidai-193-2 Yuwatsubakigawa, Akita, 010-1211 Japan

<sup>10</sup>Faculty of Environmental Earth Science, Hokkaido University, Sapporo, Japan

\*Corresponding author: ram@ees.hokudai.ac.jp; Tel.: +81-011-706-2261

### **Abstract:**

Peatlands in Indonesia are subject to subsidence in recent years, resulting in significant soil organic carbon loss. Their degradation is responsible for several environmental issues; however, understanding the causes of peatland subsidence is of prime concern for implementing mitigation measures. Here, we employed time-series Small Baseline Subset (SBAS) Interferometric Synthetic Aperture Radar (InSAR) using ALOS PALSAR-2 images to assess the relationship between subsidence rates and land use/land cover (LULC) change (including drainage periods) derived from decadal Landsat data (1972-2019). Overall, the study area subsided with a mean rate of  $-2.646 \pm 1.839$  cm/year in 2018-2019. The subsidence rates slowed over time, with significant subsidence decreases in peatlands after being drained for 9 years. We found that the long-time persistence of vegetated areas leads to subsidence deceleration. The relatively lower subsidence rates are in areas that changed to rubber/mixed plantations. Further, the potential of subsidence prediction was assessed using Random Forest (RF) regression based on LULC change, distance from peat edge, and elevation. With an  $R^2$  of 0.532 (RMSE = 0.594 cm/year), this machine learning method potentially enlarges the spatial coverage of InSAR method for the higher frequency SAR data (such as Sentinel-1) that mainly have limited coverage due to

decorrelation in vegetated areas. According to feature importance in the RF model, the contribution of LULC change (including drainage period) to the subsidence model is comparable with distance from peat edge and elevation. Other uncertainties are from unexplained factors related to drainage and peat condition, which need to be accounted for as well. This work shows the significance of decadal LULC change analysis to supplement InSAR measurement in tropical peatland subsidence monitoring programs.

**Keywords:** Peat subsidence, SBAS InSAR, LULC change, tropical peatlands, PALSAR-2, Landsat

## 1. Introduction:

Peatlands, formed from the accumulation of decomposed organic materials over millennia, are considered to be critical natural carbon sinks due to their large carbon storage capabilities (Loisel et al., 2021; Yu et al., 2010). Despite covering only 3% of the Earth's land surface, peatlands are crucial in the global carbon cycle (FAO, 2020). Their contribution to the carbon cycle is 612 Gt, and is equivalent to a quarter of the global carbon storage (Yu et al., 2010). Tropical peatlands account for 18-25% of total peatland volume, although they only contribute to 11% of total peatland area due to higher concentration of carbon (carbon stocks per area; 40-62%) than boreal peatlands (Donato et al., 2011; Page et al., 2011). South-East Asia has 43% (24.8 Mha) of tropical peatlands worldwide, where the peatlands are mostly located in Indonesia (20.7 Mha; 36%; the percentage is recalculated referring to Dargie et al., (2017)) (Hooijer et al., 2006, 2012; Page et al., 2011).

Degradation of Indonesian tropical peatlands is a major negative issue driven by human activities (e.g., deforestation, conversion to plantations, and construction) and climatic changes

(e.g., El Niño Southern Oscillation) (Bourgeau-Chavez et al., 2018; Osaki et al., 2016). Miettinen et al., (2016) reported extensive deforestation in tropical peatlands in Insular South-East Asia (i.e., Malaysian peninsula, Sumatra, and Borneo) due to the conversion to industrial plantations and small-holder areas during the period of 1990 to 2015, with the remaining forest comprising only 29% of the total area. This deforestation also includes small peat-covered islands such as Bengkalis Island (Indonesia), which lost 90% of the total area (Juniyanti et al., 2020). As a result, the peatlands emitted 2.5 Gt of carbon (146 Mt/year) during that period (Miettinen et al., 2017).

Waterlogged conditions in a pristine peatland keep anoxic states of the peat; however, when the peatland is drained, oxygen enters soil leading to oxidation (FAO, 2020). Simultaneously, peat subsidence occurs, promoting consolidation (compression of peat layers below groundwater level), biological oxidation, and soil shrinkage due to desiccation (Wösten et al., 1997). Thus, the peat subsidence rate is mainly determined by temperature and the presence of oxygen (Gambolati et al., 2005). Other key factors include peat type, rate of decomposition, density and the peat deposit thickness, drainage depth, climate, land use, and drainage period (Grzywna, 2017; Hooijer et al., 2012; Hoyt et al., 2020; Wösten et al., 1997).

The only way to halt subsidence is by rewetting the peat (Wösten et al., 1997), hence, water management plays a key role in peatlands restoration (Hooijer et al., 2012). The wetness condition of peatlands is associated with the existing land use/land cover (LULC), for instance, plantations need drainage practices that influence peatlands' wetness condition (Prastyaningsih et al., 2019). The rate of carbon loss or emission factor due to peatland degradation is also related to particular LULC types as documented by the Intergovernmental Panel on Climate Change (IPCC) (Drösler et al., 2014). The subsequent subsidence rates after a land conversion depend on

land and water management, hence subsidence rates could vary for a particular LULC class in a prolonged period although the long-term subsidence is generally constant at 5 cm/year (Hooijer et al., 2012). Hoyt et al., (2020) revealed that the carbon emissions due to peatland subsidence could not be determined only by LULC classes, but mostly related to drainage conditions, however, the long-term LULC change has not been considered. The availability of Landsat archive data since the 1970s offers a great opportunity to explore the relationship between decadal LULC change and peat subsidence rates, and potentially, at large spatial scales that would not be possible otherwise.

Peat subsidence can be measured using some terrestrial-based methods. The traditional technique is monitoring the surface change from the reference datum by anchoring poles vertically into the underlying mineral subsoil (Evanoff et al., 2019; Ichsan et al., 2013). Other measurements are the utilization of geodetic-based approaches (Dahdal, 2011; Grzywna, 2017; Reeve et al., 2013), and the Rod Surface Elevation Table–Marker Horizon (RSET-MH) method (Jaya et al., 2016; Webb et al., 2013). However, these methods are point-based and unable to represent a large area. In contrast, the Interferometric Synthetic Aperture Radar (InSAR) technique has been widely used to monitor land surface movements in a wider area more efficiently. The archived and prolonged InSAR images enable time-series monitoring with millimeter accuracy (Xue et al., 2020).

Temporal decorrelation (changes of land surface conditions) becomes the main issue in the tropical region, where volume scattering is dominant on the dense vegetation coverage (Pepe & Calò, 2017; Wei & Sandwell, 2010). Time-series InSAR can reduce decorrelation and improve signal-to-noise ratio by observing the temporal movement of land surface based on a stack of multitemporal Synthetic Aperture Radar (SAR) images (Agram & Simons, 2015). Among

numerous techniques, the two most notable approaches are Persistent Scatterer Interferometry (PS InSAR) (Ferretti et al., 2001) and Small BAseline Subset (SBAS) (Berardino et al., 2002). PS InSAR is focused on the detection of movement of stable objects such as in urban areas. SBAS InSAR uses a distributed scatterer through small spatial and short temporal baselines to maximize coherence and is also capable of detecting non-linear movements (Gheorghe & Armaş, 2016; Minh et al., 2020; Osmanoglu et al., 2016). A recent technique, Intermittent SBAS (ISBAS), was developed utilizing intermittently coherent pixels that improve the capability of InSAR measurement in low coherence areas (Sowter et al., 2013). Therefore, these approaches (SBAS and ISBAS) are more often implemented for the rural areas, including peatlands in the temperate zone (Alshammari et al., 2018; Cigna et al., 2014; Stockamp, 2018) and the tropics (Hoyt et al., 2020; Khakim et al., 2020; Marshall et al., 2018; Zhou et al., 2019). These previous studies are summarized in Table A.1.

While most of our understanding about InSAR based land subsidence monitoring is based on existing LULC, less is known about the decadal change in LULC and land subsidence as we hypothesized that there is a relationship between them (Figure 1). Therefore, this study aims to improve our knowledge to estimate the peat subsidence rate in Bengkalis Island, Indonesia, using time-series SBAS InSAR based on ALOS PALSAR-2 (Phased Array type L-band Synthetic Aperture Radar-2) data and analyze the subsidence rate with decadal LULC changes and drainage periods. LULC maps were derived from the Landsat time-series (Landsat 1, 5, and 8) images from 1972 to 2019. Furthermore, this study assesses the potential of enlarging spatial coverage of SBAS InSAR results by several parameters comprising LULC maps, distance from the edge of peatlands, and elevation data.

## 2. Study Area:

Bengkalis Island is a peat-dominated island, located 10 km from the east coast of Sumatra Island, Indonesia. Seventy-four percent (665 km<sup>2</sup>) of the total area is covered by at least 1 m deep peat deposits with a maximum thickness of 10-15 m (Supardi et al., 1993). Most peatlands in western Indonesia started to form after the Deglacial and during the Early Holocene period – these include peatlands in Bengkalis Island which were formed approximately 5,400 years ago (Dommain et al., 2014). The peat formation began with the topogenous peat deposits as a result of debris plant accumulation in the nearly flat coastal plain, then followed by the formation of domed peat, i.e., ombrogenous deposits (Supardi et al., 1993). Five peat domes lie in Bengkalis Island. Our focus is on the north-western side of the island, including Areas 1, 2, 3, 4, and a small area of Area 5 (Figure 2). The categorization is based on the peat domes in this island, referring to Supardi et al., (1993).

In recent decades, from 1990 to 2013, the forest area in Bengkalis Regency (including Bengkalis Island) has declined from 6.13 ha to 191 ha (Rijal, 2019). By 2019, only 10% of the study area was covered by forests, while industrial plantations covered most of the area (Juniyanti et al., 2020).

## 3. Materials and Methods:

The methodology of this study consists of 4 parts, i.e., peat subsidence rates estimation derived from SBAS InSAR, LULC classification and change, analysis between subsidence and drainage period as well as LULC change, and subsidence modeling using machine learning regression. The flowchart of this study is depicted in Figure 3.

### 3.1. Materials

#### 3.1.1. PALSAR-2 Data

PALSAR-2 is an L-band SAR sensor equipped on ALOS-2 satellite, working at a 1.2 GHz frequency and 23.6 cm wavelength. The L-band wavelength can minimize the errors induced by temporal and volumetric decorrelation in the vegetated area (Wei & Sandwell, 2010). This sensor provides a larger coverage of the coherent area in peatlands as compared to the higher frequency SAR data (i.e., Sentinel-1) (Alshammari et al., 2018; Cigna et al., 2014; Zhou et al., 2019). PALSAR-2 data are provided by Japan Aerospace Exploration Agency (JAXA) in Stripmap mode with level 1.1 Single Look Complex (SLC). Table 1 shows the total of 12 images acquired during the 2016-2019 period.

#### 3.1.2. Landsat Data

This study used multispectral Landsat series images, including Landsat 1 MSS (Multi Scanner System), Landsat 5 TM (Thematic Mapper), and Landsat 8 OLI (Operational Land Imager). The acquisition date expands between 1972 and 2019 to cover the decadal changes as shown in Table 2. Landsat 5 and Landsat 8 images were obtained from the Google Earth Engine (GEE) cloud computing platform. Only the cloud-free images were selected, then a cloud mask method was applied based on CFMask (C code based on the Function of Mask) algorithm (Foga et al., 2017). The datasets were corrected for surface reflectance level using LEDAPS (Landsat Ecosystem Disturbance Adaptive Processing System) method (Claverie et al., 2015; Masek et al., 2006). Since the surface reflectance level of Landsat 1 is not available on the GEE, we downloaded and processed the required data from the USGS EarthExplorer (<https://earthexplorer.usgs.gov/>).

### 3.1.3. Field Data

Groundwater level (GWL) derived subsidence rates were used to validate the SBAS InSAR results. The GWL measure can describe subsidence rate in tropical peatlands (Comeau et al., 2013; Dariah et al., 2014; Hirano et al., 2014; Hooijer et al., 2012; Husnain et al., 2014; Jauhiainen et al., 2012; Wösten et al., 1997). We measured the water table depth by blowing into a long straw in a perforated PVC tube inserted vertically through the peat surface until hearing a ‘bubbling’ sound (Hooijer et al., 2012; Ichsan et al., 2013). GWL data were collected during the field survey on 10-13 September 2019 to cover 64 points. The daily GWL data of 3 sites in the study area were acquired from SIPALAGA (Peatland Water Monitoring System), were used to calibrate the temporal change of field measurement. The location of field based GWL data and SIPALAGA sites are depicted in Figure 2.

Given that each plot's measurement time is different, the field measurement data were calibrated with SIPALAGA daily data. The SIPALAGA data of 10 September 2019 was used as the basis, then we calculated the mean differences from the SIPALAGA data of the next 3 days. The mean differences are 0.73, 1.33, and 1.73 cm respectively for the second, third, and fourth days, which were used for calibrating the field based GWL data on the corresponding day.

Further, we converted GWL data to mean annual GWL by adding the value of 28.09 cm obtained from the subtraction between daily data and the mean annual SIPALAGA data. Subsidence rates were calculated using GWL data based on the following equation derived from Hooijer et al., (2012):

$$VD = 0.69 + (0.0598 \times \text{GWL}) \quad (1)$$

where, VD is annual vertical displacement (cm/year, subsidence as negative value) and GWL (cm) is the mean annual GWL.

## 3.2. Methods

### 3.2.1. SBAS InSAR

MintPy (Miami InSAR Time-Series Software in Python) toolbox was used to process SBAS InSAR (Yunjun et al., 2019). This toolbox requires a stack of differential interferograms that have been generated using ISCE (Interferometric SAR Scientific Computing Environment) (Rosen et al., 2012). The SBAS InSAR processing is depicted in Figure 4. The steps in ISCE consist of coregistration, interferogram generation, Goldstein adaptive filtering, topographic phase removal, and phase unwrapping. We used the maximum temporal baseline of 1 year to construct the image pairs during coregistration. Multilooking was applied with a factor of 22 (azimuth looks) x 9 (range looks) to minimize speckle noise and enhance coherence (Chen et al., 2020). The topographic contribution was subtracted using 1-arc second SRTM Version 3.0 DEM data. We employed a 2D statistical-cost network-flow phase-unwrapping algorithm (SNAPHU) to unwrap the interferograms (Chen & Zebker, 2001).

The stack of unwrapped interferograms was then processed in the MintPy smallbaselineApp workflow (Yunjun et al., 2019). Correlation-based SBAS network modification was applied with a coherence of 0.7 (Chaussard et al., 2015), yet all networks have spatial coherence above the threshold (Figure 5a). A point in the center of Bengkalis City ( $1.4714^{\circ}$  N,  $102.1097^{\circ}$  E) was selected as the reference since it is considered the most stable area without displacement. Unwrapping error correction was applied with a bridging method by connecting regions with moderate to high coherence using tree searching algorithms (Yunjun et al., 2019). We set the threshold to mask the pixels having temporal coherence below 0.4.

Tropospheric phase contribution was eliminated using the estimated tropospheric delay derived from ERA-5 (Jolivet et al., 2011). Also, we applied linear phase deramping to correct phase ramps resultant from residual tropospheric and ionospheric delays. The topographic phase residual caused by elevation model error was corrected based on the proportionality with the perpendicular baselines (Fattahi & Amelung, 2013). After corrections, noise may still remain, hence an evaluation was conducted by calculating the root mean square (RMS) of the residual phase. Based on the RMS value evaluation (Figure 5b), the result of PALSAR-2 data acquired on 16/07/2016 was discarded in the velocity calculation. Because this study assumes that only vertical displacement occurred in the peatlands areas, hence, the Line of Sight (LOS) displacement for each date was converted to vertical displacement by dividing it with the cosine of incidence angle. Vertical velocity was computed by the linear fit on the vertical displacement images with the start dates on 13/02/2016 (initial observation date) and 01/27/2018 (starting from 2018), and the same end dates, i.e., 24/08/2019. The 2018 shorter-time calculation was also considered, as a recent study used a shorter time span of SBAS InSAR processing (Khakim et al., 2020). We then evaluated the vertical velocity results using the GWL based annual subsidence.

### 3.2.2. LULC Classification

Land use/land cover (LULC) classes used in this study are built-up areas, cleared/burned land, shrub, oil palm plantations, rubber/mixed plantations, forest (secondary and primary), water, and mangroves. These classes refer to a previous study by Crowson et al., (2019) with some adjustments considering the local conditions in the study area.

We added several image transformations for the classification input to improve the results, consisting of the Normalized Difference Vegetation Index (NDVI) (Rouse et al., 1974),

Mangrove Vegetation Index (MVI) (Baloloy et al., 2020), and Normalized Burn Ratio (NBR) (Key & Benson, 2005). The image transformations were calculated using the following equations:

$$NDVI = \frac{(NIR-Red)}{(NIR+Red)} \quad (2)$$

$$NBR = \frac{(NIR-SWIR2)}{(NIR+SWIR2)} \quad (3)$$

$$MVI = \frac{(NIR-Green)}{(SWIR1-Green)} \quad (4)$$

Since SWIR bands are not available for Landsat 1, we did not include NBR, and replaced MVI with Normalized Difference Wetness Index (NDWI) (Gao, 1996). The equation of NDWI is as follows:

$$NDWI = \frac{(Green-NIR)}{(Green+NIR)} \quad (5)$$

We referred to the Indonesian topographic map of 1977 (1:100,000) for the selection of training samples of the Landsat 1972 data, due to the limited interpretability from its lower spatial and spectral resolution. This topographic map was also used to help interpret the 1988 and 1998 Landsat images. Google Earth image was used to assist the interpretation of 2010 and 2019 Landsat images, while a mosaic of SPOT images (dated in 2013) provided by the Indonesian Geospatial Agency was utilized for interpreting the 2015 Landsat image. Some training samples are also based on the field visit (10-13 September 2019) for the 2019 image. The training samples are well distributed in the study area, with the number corresponding to the area of each LULC (Cheng et al., 2018).

A traditional machine learning algorithm-based Support Vector Machine (SVM) was applied to classify the LULC using DZetsaka plugin in QGIS, based on the scikit-learn library (Karasiak, 2019). The SVM approach is a supervised learning model primarily used for non-

parametric classification to handle high-dimensional data (Vapnik, 2000). In such LULC classification cases using satellite imagery, SVM has comparable performance to Random Forest classifier and deep learning-based methods (Kadavi & Lee, 2018; Liu et al., 2017; Mansaray et al., 2020). This algorithm is also capable of avoiding an over-fitting problem (Bahari et al., 2014).

Accuracy assessment was carried out by confusion matrix and weighted F1 score. Sample points were selected using stratified random sampling in AcAriaMa toolbox (QGIS plugin) (Llano, 2019; Olofsson et al., 2014). A total of 511-512 samples for each image were interpreted and assigned to the corresponding LULC class using the same method for training sample selection.

### **3.2.3. Associating Vertical Velocity with Drainage Period and LULC**

The effect of decadal changes of LULC was analyzed by relating them to vertical velocity. We resampled the resolution of LULC maps to 90x90 m to match the pixel size and extent of the vertical velocity image. All pixels were extracted with the values of those parameters. We excluded the peat burst area in the northern tip of the island since it is caused by an external source, i.e., coastal erosion. Water and mangrove areas were also masked in this analysis.

We firstly examined the vertical velocity of the current LULC (2019) for different drainage periods. Mann-Whitney U-test was used to see if the peat subsidence in the earlier drainage period is significantly lower than the later period for the particular LULC class. This non-parametric test identifies the differences in central tendency between two independent samples (Feltovich, 2003). In this first analysis, we did not consider the changes of LULC yet. The drainage period refers to the time when deforestation occurred by considering the change of forested areas. According to LULC maps, a drainage period map was generated representing the

age: (I) drained between 1972 and 1988 (47-31 years); (II) between 1988 and 1998 (21-31 years); (III) between 1998 and 2010 (9-21 years); (IV) between 2010 and 2015 (4-9 years); and (V) between 2015 and 2019 (4-0 years). Second, we included the decadal LULC change in the analysis of vertical velocity by calculating the mean value of each LULC change. This analysis was to understand the effect of the transformation and the persistence of LULC on peat subsidence.

### **3.2.4. Vertical Velocity Modeling**

To explore the potential of prediction, we used a Random Forest (RF) regression approach using the reference of vertical velocity produced by SBAS InSAR and the inputs comprising LULC change (1972, 1988, 1998, 2010, 2015, and 2019), distance from peat edge, and elevation data. As the peatlands have a dome shape, the parameters of distance from peat edge and elevation are associated with peat thickness which is one of the factors describing subsidence rates (Hoyt et al., 2020; Rudiyanto et al., 2018). Distance from the peat edge was calculated based on Euclidean distance, while the elevation data is from a high-resolution (0.27-arcsecond) Indonesian digital surface model (namely DEMNAS) acquired through InSAR processing in 2013. A previous study unveiled the vertical velocity derived from ALOS PALSAR-1 data at a regional scale using LULC data (1990 and 2007) and distance from peat edge (Hoyt et al., 2020). In this study, we extended the LULC data to cover the earliest condition that can be captured by optical satellite data (1972) with decadal change. We processed the RF algorithm using EnMAP-Box in QGIS software (van der Linden et al., 2015). The total samples (61,414 pixels) were split: 70% of samples for training and the rest for testing. The 30% of validation samples refers to the percentage of decorrelated areas resulted from previous studies using C-band SAR data (ERS and Sentinel-1) in order to observe the potential of covering the incoherent areas when the

similar time-series InSAR method is applied using higher frequency SAR data (Umarhadi et al., 2021).

We set a hyperparameter grid with different numbers of trees (ntrees) (i.e. 100, 200, 500, and 1,000) where the model selection was implemented through GridSearchCV (Grid Search with Cross Validation;  $CV = 3$ ). The best estimator was chosen based on the coefficient of determination ( $R^2$ ) value. We evaluated the learning performance using 10-fold cross-validation, then tested the results by assessing root mean square error (RMSE). To compare the significance of each variable to the model, mean decrease in impurity (MDI) feature importances were computed based on totally randomized trees in asymptotic conditions (Louppe et al., 2013).

## 4. Results

### 4.1. Peatland Subsidence

Figure 6 illustrates the vertical displacement of each PALSAR-2 data based on SBAS InSAR processing. Eighty-eight pixels or 0.68% of the study area cannot be characterized using a coherence threshold of 0.4. Other than the initial image, land subsidence dominated the study area. Although corrections on tropospheric delay, phase ramp, and topographic residual have been performed, the residual phase remained. Based on the RMS calculation in Figure 5b, the displacement image of 16/07/2016 was discarded for velocity calculations, showing the apparent phase ramps in the western part of that image (Figure 6).

Vertical velocity (cm/year) was calculated based on the first acquisition date (13/02/2016) and 2018 (27/01/2018). Figures 7a-b depict the difference between the vertical velocity of the two images. In the subsidence area, the depression rates calculated from 2018 are higher than from 2016. Vertical velocity is based on the slope of the best fitting line to the displacement time

series. As shown in Figure 6, the significant subsidence is detected in the latest date (24/08/2019), hence the shortening calculation period (from 2018) is more affected by the displacement values of the last observation date.

We evaluated the vertical velocities calculated from the two different starting dates using GWL based annual subsidence by plotting the scatterplots as shown in Figures 7c-d. Out of 64 field data that we collected, only 47 data that we used due to decorrelation in InSAR result. The vertical velocity calculated from 2018 has a higher coefficient of determination and lower RMSE value with GWL based annual subsidence ( $R^2 = 0.263$ ,  $p < 0.05$ ,  $RMSE = 1.383$  cm/year) in comparison to the vertical velocity with the initial date of 2016 ( $R^2 = 0.098$ ,  $p < 0.05$ ,  $RMSE = 1.415$  cm/year). It shows that the vertical velocity calculated from 2018 is more accurate than the calculation from 2016 to represent the ground data. Therefore, we used the vertical velocity calculation from 2018 for the analysis with LULC change (Subsection 4.3) and modeling (Subsection 4.4).

Based on the estimated vertical velocity, we observed that almost the whole study area experienced land subsidence. Without including the non-peat area, the average vertical velocity is  $-2.646 \pm 1.839$  cm/year. Uplifts are also detected in the built-up and cleared areas in the northern part with a maximum value of 4.416 cm/year. As per peat areas, the mean velocities are  $-3.505 \pm 3.332$ ,  $-3.087 \pm 2.134$ ,  $-2.348 \pm 1.402$ , and  $-2.324 \pm 1.373$  cm/year respectively, in Areas 1, 2, 3, and 4. Significant subsidence areas are recorded in the north-western tip (Area 1), with the highest rate of  $-17.416$  cm/year, due to the bog bursts. This phenomenon is induced by coastal erosion and peat landslide that causes the peat flowing out to the sea at a rapid rate (Yamamoto et al., 2019).

## 4.2. LULC Classification and Transformation

The results of the LULC classifications are shown in Figure 8a and the area in percentage is presented in Table 3. In 1972, almost half (48.43%; 272.13 km<sup>2</sup>) of the study area was still covered by forests. There were no oil palm plantations detected in this first observation period, yet deforestation had occurred as evidenced by the cleared/burned areas (13.85%), shrubs (8.66%), and rubber/mixed plantations (21.69%) in the vicinity of the forest edge. Subsequently, deforestation gradually increased in the following decades, leading to 15.43 km<sup>2</sup> (2.75%) forest coverage remaining in 2015. In 2019, the forest area slightly increased in the south-eastern side of the study area (Figure 8a).

Oil palm plantations started to grow in 1988 with an area of 3.41 km<sup>2</sup> (0.61%). The oil palm plantation area continuously expanded to 31.12% of the total area in 2019. Rubber/mixed plantations covered 36.95% of the total area in 2010 and remained the largest LULC class (33.93% coverage, 2019). Shrub area increased significantly to 34.23% in 1988 and gradually decreased in the following decades and was replaced by plantations. In general, shrubs are in the transition between forests and plantations, as the low vegetation grew after the forests were cut and removed.

Spatially, significant deforestation occurred in Areas 3 and 4 as observed in 1988 and 1998. This is followed by the growth of oil palm plantations in the eastern side of the study area. During the period between 1998 and 2010, large areas were deforested, particularly in Areas 1 and 2. Nearly Areas 1 and 2 were replaced by oil palm plantations (Figure 8a). Forests in Area 3 represent <50% of the previously forested area.

Based on the confusion matrices (Tables A.2-A.7), our results achieved an overall accuracy of >80% for all classifications (Table 3, Table A.8). The weighted F1 score of each year show

somewhat similar to overall accuracy, reconfirming the accuracy of the classification results. Even though Landsat 1 has fewer bands (four bands) and a lower spatial resolution (60 m), the accuracy is comparable to the other classification results derived from Landsat 5 and 8. This is mainly because of the absence of oil palm plantations in 1972. The spectral signature of oil palm plantations is similar to other vegetated lands (rubber/mixed plantations and forest) and shrubs due to several factors, including forest age and management priority (presence of understory vegetation). These differences can cause some misclassifications in the 1988-2019 images.

#### **4.3. Relationship Between Subsidence and Drainage Periods Well as LULC**

We calculated the mean vertical velocity corresponding to recent LULC types for the whole area as well as the drained area before 1972 and after 1972 based on the forest area of the 1972 map (dashed lines in Figure 9a). Regardless of the drainage period, oil palm (-3.250 cm/year) subsided at a higher rate than other LULC classes (Mann-Whitney U-test;  $p < 0.05$ ), followed by shrub and forest classes. The separation of the general drainage period clearly shows the difference that vertical velocity in the area drained before 1972 is much slower than after 1972 in all LULC classes. The forest subsided more in the area drained after 1972 (Figure 9a). Comparatively, rubber/mixed plantations show relatively low subsidence.

To further evaluate the effects of the drainage period, we divided the drained area after 1972 into 5 periods. The bar graph in Figure 9a describes the mean values of the vertical velocity of the recent (2019) LULC map calculated from each drainage period, while the significance of decelerated subsidence is shown in Figure 9b. Cleared/burned area, oil palm, and rubber/mixed plantations show a significant decrease of subsidence rate along with the older drainage time in the first three periods (9-47 years), although the difference between Period II and Period III in cleared/burned area is not significant. The rates in the forest are quite similar across the drainage

period (-3.224 to -3.622 cm/year). The shrub class does not show clear trends, yet there are significant decreases after Period II (Figure 9b).

We further quantified mean subsidence rates considering the change of LULC (Table 4). Our focus is on the unaltered LULC classes in the following observation period(s) after the conversion. In general, those classes changed in the earlier periods (from 1988 and 1998) have lower subsidence rates than in recent changes. The subsidence rates of areas changed to rubber/mixed plantations are relatively lower, which are followed by the reforested areas in 1988 and 1998. Reforested area in Table 4 is represented by the non-forest area that changed to forest in the following year(s). However, the more recent reforestation (2010 and 2015) are not lower than the others. A notable contrast is observed for oil palm plantations, where the plantations converted in 1998 subsided much slower than the young plantations. In contrast, the differences are not clear for the areas changed to cleared/burned and shrub. The changes from the forest clearly show that the subsidence is higher as the ground area is more exposed (cleared/burned, shrub, and oil palm). While the revegetated areas (oil palm, rubber/mixed plantations, and forest) from cleared/burned areas in the recent period subsided at a high rate.

In the LULC change matrix (Table 4), the subsidence rates of the unchanged LULC types are apparent. As already mentioned, the subsidence rates of older oil palms are lower than the younger oil palms, along with unchanged oil palm areas. The persistent forest areas subsided at a higher rate than the unchanged rubber/mixed plantations, even though the forests that were intact since 1988 (-3.224 cm/year).

#### **4.4. Vertical Velocity Estimated from RF Regression**

Before processing the model, we assessed the relationship between vertical velocity and distance from peat edge as well as elevation. Figure 10 shows the scatterplots of these

parameters, depicting the coefficient of determination of 0.312 ( $p < 0.05$ ) and 0.332 ( $p < 0.05$ ), respectively.

Based on the GridSearchCV model selection, the best estimator is the model with 1,000 trees ( $R^2 = 0.532$ ). It shows that 53.20% of the vertical velocity can be explained by these parameters. MDI feature importances were calculated, resulting in the ratio of 0.338, 0.299, and 0.363 for, respectively, LULC change, distance from peat edge, and elevation. Figure 11a depicts the image of modeled vertical velocity. The model produced a relatively small error with an RMSE of 0.594 cm/year calculated from 18,424 testing samples. The scatterplot between the modeled vertical velocity and SBAS InSAR of testing samples is illustrated in Figure 11b.

Visually, the image of SBAS InSAR result (Figure 7b) and vertical velocity model (Figure 11a) are fairly similar; however, some pixels are quite different. To delineate differences, profile lines (Figure 11c) are plotted on the 3 peat areas. Thus, Profiles A, B, and C represent respectively, Areas 2, 3, and 4. The profile lines show that the values are not precisely the same, yet, they have the same pattern without significant variances. The highest contrast is in the middle of Profile B, with a difference of 2.720 cm/year.

## 5. Discussion

### 5.1. Peat Subsidence Estimation by SBAS InSAR

By setting a coherence threshold of 0.4, the SBAS InSAR processing could cover almost the whole of the study area, although this threshold is higher than the previous studies (i.e., 0.2-0.25) using Sentinel-1 C-band and ALOS PALSAR (Khakim et al., 2020; Marshall et al., 2018; Zhou et al., 2019). L-band PALSAR-2 has the advantage of having a higher coherence in a vegetated area compared to the X and C-band SAR sensors such as TerraSAR-X, Radarsat-1/2,

and Sentinel-1. However, temporal-resolution is a limitation of the PALSAR-2 data since only few images are available for a particular area in a given period, although the designed revisit time is 14 days. For instance, in our study area, only 12 images are available between 2016-2019, of these images four have a gap of more than 150 days. The image number of ScanSAR mode acquired by PALSAR-2 is more than the Stripmap mode (used in this study), with a wider swath to cover a larger area. However, this mode has a coarser resolution, i.e., 100 m (WD1) and 60 m (WD2). Future studies can evaluate the implementation of ScanSAR acquisition mode of PALSAR-2 in tropical peatlands and combine it with Stripmap mode (Park et al., 2020).

Our SBAS InSAR result has an  $R^2$  of 0.263 ( $p < 0.05$ ) and an RMSE value of 1.383 cm/year using the reference of GWL based annual subsidence. Hooijer et al., (2015) reported that although several studies found a strong correlation between GWL and subsidence, some of them also observed a low correlation, hence GWL based subsidence data does not completely represent the actual condition. Validation of subsidence derived from InSAR techniques in tropical peatlands is still challenging, even more in a peat-dominated island like our study area. As summarized in Table A.1, because of lack of data, no studies used the ideal long-term GNSS data for validating time-series InSAR based peat subsidence in South-East Asia. The recent study validated the results by calculating the stable points in a non-peatland area (>15 km away from peat edge) (Hoyt et al., 2020). It cannot be achieved in this study because the most considered stable area (in the city center) is in the transition area that is very close to the peat edge (<2 km). We recommend the combination of GNSS station data with long-term (SIPALAGA data in Indonesia) and short-term (field measurement) GWL data would improve the quality of validation.

The results show that subsidence rates in Area 2 are higher than Areas 3 and 4 (Figure 7b) due to the more recent drainage period and domination of oil palm plantations in this area. The mean velocity of Area 2 is  $-3.087 \pm 2.134$  cm/year, while Areas 3 and 4 are  $-2.348 \pm 1.402$  and  $-2.324 \pm 1.373$  cm/year, respectively. Our results are consistent with similar InSAR-based peat subsidences with a reported mean rate of  $-2.2$  cm/year (Hoyt et al., 2020), and field measurement by Wösten et al., (1997) ( $-2$  cm/year), yet it is below the long-term subsidence rate ( $-5$  cm/year) measured by Hooijer et al., (2012). The subsidence in about half of Area 1 is mostly affected by the peat burst driven by coastal erosion. The eroded peatlands then formed a secondary decomposition sandwiched with clay layers in an anaerobic condition (Yamamoto et al., 2019). Nonetheless, this phenomenon has the potential of carbon accumulation, annually accounting for  $7.4 \times 10^3$  tC/km<sup>2</sup> (Yamamoto et al., 2019), becoming worth exploring for future studies.

## 5.2. Peat Subsidence Relationship with Degradation Period and LULC Change

The decadal LULC maps revealed that the degradation of peatlands in the study area occurred immensely. The first reported driver is the Forest Use Management Agreement issued in 1986 by the government to divide all forest areas in Riau province (including Bengkalis Island) into forest concession areas (to be developed for oil palm and industrial forest plantations) (Juniyanti et al., 2020). The political situation also worsened as the weak state control caused uncontrolled substantial illegal logging in 1999-2005 by local people. They later registered the lands, then sold them to local elites (i.e., political elites, business elites, cultural elites, and bureaucratic elites) for larger-scale plantations (McCarthy, 2010; Purnomo et al., 2019). As a result, forests that covered 48.4% of the total area in 1972, only remained 3.3% in 2019. Therefore, along with excessive resource use, the lack of governance has led to an exponential degradation of forests in Bengkalis Island.

We examined the association of vertical velocity with recent LULC (2019) and drainage period as well as with the LULC change. By dividing 'before 1972' and 'after 1972', the impact of drainage time is apparent, showing that the subsidence in the area drained before 1972 has slowed down (Figure 9). The more detailed separation to include the decadal drainage period show the clear trends only for the periods older than 9 years for oil palm and rubber/mixed plantations (Table 4). A previous study reported that peat surface can collapse up to 142 cm in the first 5 years after drainage, with 75 cm lowering in the first year (Hooijer et al., 2012). This substantial subsidence is not found for the latest drainage period (Period V) because the surrounding forest area has already been drained some years before our SAR observation date. As observed in the field, although covered by forest, the GWL is far below the surface (direct GWL observation = -64.7 cm, mean annual GWL = -34.9 cm). The low GWL in forest area is relevant to the understanding that drainage condition in plantation areas affects the adjacent forests (Hooijer et al., 2014), even for pristine forests (Evans et al., 2019).

Overall, the subsidence in reforested areas (after being drained) and the intact forests do not have significantly lower rates (Table 4). The term of intact forests is the areas where forests did not change to other LULC classes from 1988 to 2019. The rates are higher even in the newly reforested area between 2015 and 2019 compared to those changed to rubber/mixed plantations. As mentioned before, this is due to the dry condition of peat soil due to drainage canals in the surroundings. The interchanges between rubber/mixed plantations and forest show relatively lower subsidences among the others. We found that the drainage canals in rubber/mixed plantations are less dense than in oil palm plantations, which may be the reason that the transition to rubber/mixed plantations subsided slower than oil palm plantations. Mechanical compaction on the harvesting paths and planting rows using heavy machinery also contributes to

high subsidence in oil palm plantations during land preparation (Lewis et al., 2020; Othman et al., 2009). The compaction allows accessibility and improves palm growth through increased bulk density. Furthermore, we observed that the LULC persistence may lead to the decrease of subsidence rates, showing by the lower subsidence in the areas where were changed in the earlier periods (i.e., changed from LULC 1988 and 1998) than the recent changes. It is mainly because a LULC conversion or plantation rotation is initiated by land clearing, land management, or even fires leading to mechanical compaction (Evans et al., 2019).

Mixed/rubber plantations seem to be the most sustained LULC type compared to the other classes, however, the only way to halt the subsidence rate is through a rewetting practice (Wösten et al., 1997). This cannot be afforded by this type of plantation, which needs a dry condition (Prastyaningsih et al., 2019). Wet agriculture practice (paludiculture) is promoted these years, becoming the best solution since it works in two ways at once, i.e., restoring the peatland ecosystem and providing economic values (Budiman et al., 2020; Prastyaningsih et al., 2019; Tan et al., 2021). This practice can also help prevent the dry condition in forest areas through the implementation of canal blockings and soil rewetting in the surrounding forests (Budiman et al., 2020). Yet, this is still a big challenge to involve both the local people and the companies that are engaged in industrial plantations (Baffoni et al., 2017).

We only identified general LULC classes as a trade-off of taking advantage of long archive medium-resolution Landsat data. Sentinel-2 data, with 10 m spatial resolution, would be worthy of consideration to provide more detailed LULC classes, including paludiculture-based vegetation types that were not explored in this study. Thus, the detailed classification can help the monitoring of restoration activity.

### 5.3. Potential of Machine Learning to Predict Peat Subsidence

According to the coefficient of determination, peat edge ( $R^2 = 0.321$ ) and elevation ( $R^2 = 0.332$ ) are potential to explain the variation in vertical velocity, hence these two parameters were evaluated in the study. Further, feature importances were assessed in the RF model, showing that the contribution of LULC change (including drainage period) to vertical velocity accounted nearly equal (MDI = 0.338) to other two parameters: distance from peat edge (MDI = 0.299) and elevation (MDI = 0.363). Although not directly representing the actual peat condition, the approach of distance from peat edge and elevation can be used for associating with peat subsidence.

We examined the potential of vertical velocity prediction by applying RF regression between SBAS InSAR result and the parameters consisting of decadal LULC changes (1972 to 2019), proximity to peat edge, and elevation. The modeling result shows that about half (53.20%) of the vertical velocity can be explained by the parameters based on the coefficient of determination. More than 40% of the vertical velocity variation might come from the other important factors that were not considered in this study, including drainage condition (proximity, drainage depth, and canal maintenance) (Hooijer et al., 2014) as well as peat type, organic matter decomposition rate, and peat deposit thickness and density (Grzywna, 2017). Also, our LULC maps have around a decade gap. The interval shortening of LULC maps increases the number of learning variables that can improve the modeling results. However, our traditional machine learning procedure can reach relatively low error (RMSE = 0.594 cm/year). In the future, this combination of time-series InSAR and machine learning methods can be applied to cover the uncharacterized areas due to the decorrelation problem in the vegetated peatland area. For instance, in tropical peatlands, the incoherent area based on Sentinel-1 is 30% of the total land

area (Umarhadi et al., 2020), while another study reported only 62% coverage for the coherent area despite using ALOS PALSAR data (Zhou et al., 2019).

## 6. Conclusion

This study showed that peat-dominated Bengkalis Island is subsiding in a range of long-term peat subsidence (mean =  $-2.646 \pm 1.839$  cm/year), except in the northern tip of the island where significant subsidence is driven by peat burst. We spatially proved the previous studies that the longer drainage period contributes to the deceleration of subsidence rates, with the significant differences in the period >9 years after being drained for oil palm and mixed/rubber plantations. The slowing rates are also apparent for the persistent vegetation-covered LULC types (oil palm, mixed/rubber plantations, and forest). Rubber/mixed plantations maintained the relatively lower subsidence compared to other LULC classes, nevertheless, these plantations do not stop the subsiding peat – only reweaving practice does. Further, we revealed the potential of decadal LULC maps, distance from the peat edge, and elevation to predict vertical velocity through RF regression with an RMSE of 0.594 cm/year. This machine learning method shows the potential of spatial coverage enlargement to cover the decorrelated areas which may occur in the vegetated area of tropical peatlands.

## Acknowledgment

We would like to thank JAXA for providing PALSAR-2 data (RA-2: PER2A2N133), and Peatland Restoration Agency (BRG) of Indonesia for the availability of SIPALAGA data. Landsat images are freely provided by USGS. Authors thank M.Z. Afwani for his help during the

field survey. The first author would like to acknowledge the financial support from MEXT-Monbukagakusho, Japan scholarship.

## References

- Agram, P. S., & Simons, M. (2015). A noise model for InSAR time series. *Journal of Geophysical Research: Solid Earth*, *120*(4), 2752–2771.  
<https://doi.org/10.1002/2014JB011271>
- Alshammari, L., Large, D., Boyd, D., Sowter, A., Anderson, R., Andersen, R., & Marsh, S. (2018). Long-Term Peatland Condition Assessment via Surface Motion Monitoring Using the ISBAS DInSAR Technique over the Flow Country, Scotland. *Remote Sensing*, *10*(7), 1103. <https://doi.org/10.3390/rs10071103>
- Baffoni, S., Miettinen, O., Tinhout, B., Separtinah, W., & Haggith, M. (2017). *Too Much Hot Air—The failure of the Indonesian pulp and paper industry to reform its management of peatlands*. Environmental Paper Network. <https://environmentalpaper.org/wp-content/uploads/2019/10/Too-much-hot-air-20170426.pdf>
- Bahari, N. I. S., Ahmad, A., & Aboobaider, B. M. (2014). Application of support vector machine for classification of multispectral data. *IOP Conference Series: Earth and Environmental Science*, *20*, 012038. <https://doi.org/10.1088/1755-1315/20/1/012038>
- Baloloy, A. B., Blanco, A. C., Sta. Ana, R. R. C., & Nadaoka, K. (2020). Development and application of a new mangrove vegetation index (MVI) for rapid and accurate mangrove mapping. *ISPRS Journal of Photogrammetry and Remote Sensing*, *166*, 95–117.  
<https://doi.org/10.1016/j.isprsjprs.2020.06.001>

- Berardino, P., Fornaro, G., Lanari, R., & Sansosti, E. (2002). A new algorithm for surface deformation monitoring based on small baseline differential SAR interferograms. *IEEE Transactions on Geoscience and Remote Sensing*, *40*(11), 2375–2383. <https://doi.org/10.1109/TGRS.2002.803792>
- Bourgeau-Chavez, L. L., Endres, S. L., Graham, J. A., Hribljan, J. A., Chimner, R. A., Lillieskov, E. A., & Battaglia, M. J. (2018). Mapping Peatlands in Boreal and Tropical Ecoregions. In *Comprehensive Remote Sensing* (pp. 24–44). Elsevier. <https://doi.org/10.1016/B978-0-12-409548-9.10544-5>
- Budiman, I., Bastoni, Sari, E. N., Hadi, E. E., Asmaliyah, Saahaan, H., Januar, R., & Hapsari, R. D. (2020). Progress of paludiculture projects in supporting peatland ecosystem restoration in Indonesia. *Global Ecology and Conservation*, *23*, e01084. <https://doi.org/10.1016/j.gecco.2020.e01084>
- Chaussard, E., Bürgmann, R., Fattahi, H., Nadeau, R. M., Taira, T., Johnson, C. W., & Johanson, I. (2015). Potential for larger earthquake in the East San Francisco Bay Area due to the direct connection between the Hayward and Calaveras Faults: The Hayward and Calaveras connection. *Geophysical Research Letters*, *42*(8), 2734–2741. <https://doi.org/10.1002/2015GL063575>
- Chen, C. W., & Zebker, H. A. (2001). Two-dimensional phase unwrapping with use of statistical models for cost functions in nonlinear optimization. *Journal of the Optical Society of America A*, *18*(2), 338. <https://doi.org/10.1364/JOSAA.18.000338>
- Chen, Y., Qiao, S., Zhang, G., Xu, Y. J., Chen, L., & Wu, L. (2020). Investigating the potential use of Sentinel-1 data for monitoring wetland water level changes in China's Momoge National Nature Reserve. *PeerJ*, *8*, e8616. <https://doi.org/10.7717/peerj.8616>

- Cheng, Y., Yu, L., Xu, Y., Lu, H., Cracknell, A. P., Kanniah, K., & Gong, P. (2018). Mapping oil palm extent in Malaysia using ALOS-2 PALSAR-2 data. *International Journal of Remote Sensing*, 39(2), 432–452. <https://doi.org/10.1080/01431161.2017.1387309>
- Cigna, F., Sowter, A., Jordan, C. J., & Rawlins, B. G. (2014). *Intermittent Small Baseline Subset (ISBAS) monitoring of land covers unfavourable for conventional C-band InSAR: Proof-of-concept for peatland environments in North Wales, UK* (C. Notarnicola, S. Paloscia, & N. Pierdicca, Eds.; p. 924305). <https://doi.org/10.1117/12.20077604>
- Claverie, M., Vermote, E. F., Franch, B., & Masek, J. G. (2015). Evaluation of the Landsat-5 TM and Landsat-7 ETM+ surface reflectance products. *Remote Sensing of Environment*, 169, 390–403. <https://doi.org/10.1016/j.rse.2015.08.032>
- Comeau, L., Hergoualc'h, K., Smith, J. U., & Verchot, L. (2013). *Conversion of intact peat swamp forest to oil palm plantation: Effects on soil CO<sub>2</sub> fluxes in Jambi, Sumatra*. Center for International Forestry Research (CIFOR). <https://doi.org/10.17528/cifor/004119>
- Crowson, M., Warren - Thomas, F., Hill, J. K., Hariyadi, B., Agus, F., Saad, A., Hamer, K. C., Hodgson, J. A., Kartika, W. D., Lucey, J., McClean, C., Nurida, N. L., Pratiwi, E., Stringer, L. C., Ward, C., & Pettoirelli, N. (2019). A comparison of satellite remote sensing data fusion methods to map peat swamp forest loss in Sumatra, Indonesia. *Remote Sensing in Ecology and Conservation*, 5(3), 247–258. <https://doi.org/10.1002/rse2.102>
- Dahdal, B. (2011). *The use of interferometric spaceborne radar and GIS to measure peat subsidence in Indonesia* [Doctoral dissertation]. University of Leicester.

- Dargie, G. C., Lewis, S. L., Lawson, I. T., Mitchard, E. T. A., Page, S. E., Bocko, Y. E., & Ifo, S. A. (2017). Age, extent and carbon storage of the central Congo Basin peatland complex. *Nature*, *542*(7639), 86–90. <https://doi.org/10.1038/nature21048>
- Dariah, A., Marwanto, S., & Agus, F. (2014). Root- and peat-based CO<sub>2</sub> emissions from oil palm plantations. *Mitigation and Adaptation Strategies for Global Change*, *19*(6), 831–843. <https://doi.org/10.1007/s11027-013-9515-6>
- Dommain, R., Couwenberg, J., Glaser, P. H., Joosten, H., & Suryadi, I. N. N. (2014). Carbon storage and release in Indonesian peatlands since the last deglaciation. *Quaternary Science Reviews*, *97*, 1–32. <https://doi.org/10.1016/j.quascirev.2014.05.002>
- Donato, D. C., Kauffman, J. B., Murdiyarso, D., Kurnianto, S., Stidham, M., & Kanninen, M. (2011). Mangroves among the most carbon rich forests in the tropics. *Nature Geoscience*, *4*(5), 293–297. <https://doi.org/10.1038/ngeo1123>
- Drösler, M., Verchot, L. V., Freibauer, A., Pan, G., Evans, C. D., Bourbonniere, R. A., Alm, J. P., Page, S., Agus, F., Hergoualc'h, K., Couwenberg, J., Jauhiainen, J., Sabiham, S., Wang, C., Srivastava, N., Bourgeau-Chavez, L., Hooijer, A., Minkkinen, K., French, N., ... Larkin, N. (2014). Drained inland organic soils. In T. Hiraishi, T. Krug, K. Tanabe, N. Srivastava, B. Jan sranjav, M. Fukuda, & T. Troxler (Eds.), *2013 Supplement to the 2006 IPCC Guidelines for National Greenhouse Gas Inventories: Wetlands*. Intergovernmental Panel on Climate Change (IPCC).
- Evans, C. D., Williamson, J. M., Kacaribu, F., Irawan, D., Suardiwerianto, Y., Hidayat, M. F., Laurén, A., & Page, S. E. (2019). Rates and spatial variability of peat subsidence in Acacia plantation and forest landscapes in Sumatra, Indonesia. *Geoderma*, *338*, 410–421. <https://doi.org/10.1016/j.geoderma.2018.12.028>

- FAO. (2020). *Peatlands mapping and monitoring – Recommendations and technical overview*.  
FAO. <https://doi.org/10.4060/ca8200en>
- Fattahi, H., & Amelung, F. (2013). DEM Error Correction in InSAR Time Series. *Geoscience and Remote Sensing, IEEE Transactions On*, 51(7), 4249–4259.  
<https://doi.org/10.1109/TGRS.2012.2227761>
- Feltoovich, N. (2003). Nonparametric Tests of Differences in Medians: Comparison of the Wilcoxon–Mann–Whitney and Robust Rank-Order Tests. *Experimental Economics*, 6(3), 273–297. <https://doi.org/10.1023/A:1026273319211>
- Ferretti, A., Prati, C., & Rocca, F. (2001). Permanent scatterers in SAR interferometry. *IEEE Transactions on Geoscience and Remote Sensing*, 39(1), 8–20.  
<https://doi.org/10.1109/36.898661>
- Foga, S., Scaramuzza, P. L., Guo, S., Zhu, Z., Dilley, R. D., Beckmann, T., Schmidt, G. L., Dwyer, J. L., Joseph Hughes, M., & Laue, B. (2017). Cloud detection algorithm comparison and validation for operational Landsat data products. *Remote Sensing of Environment*, 194, 379–390. <https://doi.org/10.1016/j.rse.2017.03.026>
- Gambolati, G., Putti, M., Teatini, P., Camporese, M., Ferraris, S., Stori, G. G., Nicoletti, V., Silvestri, S., Rizzotto, F., & Tosi, L. (2005). Peat land oxidation enhances subsidence in the Venice watershed. *Eos, Transactions American Geophysical Union*, 86(23), 217.  
<https://doi.org/10.1029/2005EO230001>
- Gao, B.-C. (1996). NDWI—A normalized difference water index for remote sensing of vegetation liquid water from space. *Remote Sensing of Environment*, 58(3), 257–266.

- Gheorghe, M., & Armaş, I. (2016). Comparison of Multi-Temporal Differential Interferometry Techniques Applied to the Measurement of Bucharest City Subsidence. *Procedia Environmental Sciences*, 32, 221–229. <https://doi.org/10.1016/j.proenv.2016.03.027>
- Grzywna, A. (2017). The degree of peatland subsidence resulting from drainage of land. *Environmental Earth Sciences*, 76(16), 559. <https://doi.org/10.1007/s12665-017-6869-1>
- Hirano, T., Kusin, K., Limin, S., & Osaki, M. (2014). Carbon dioxide emissions through oxidative peat decomposition on a burnt tropical peatland. *Global Change Biology*, 20(2), 555–565. <https://doi.org/10.1111/gcb.12296>
- Hooijer, A., Page, S., Jauhiainen, J., Lee, W. A., Lu, X. X., Morris, A., & Anshari, G. (2012). Subsidence and carbon loss in drained tropical peatlands. *Biogeosciences*, 9(3), 1053–1071. <https://doi.org/10.5194/bg-9-1053-2012>
- Hooijer, A., Page, S., Navratil, P., Vernimmen, R., van der Vat, M., Tansey, K., Konecny, K., Siegert, F., Balhorn, U., & Mawdsley, N. (2014). *Carbon emissions from drained and degraded peatland in Indonesia and emission factors for measurement, reporting and verification (MRV) of peatland greenhouse gas emissions – a summary of KFCP research results for practitioners*. LAFCP.
- Hooijer, A., Silvius, M., Mösten, H., & Page, S. (2006). *PEAT-CO2, Assessment of CO2 emissions from drained peatlands in SE Asia*. Delft Hydraulics report Q3943 (2006).
- Hooijer, A., Vernimmen, R., Mawdsley, N., Page, S., Mulyadi, D., & Visser, M. (2015). *Assessment of impacts of plantation drainage on the Kampar Peninsula peatland, Riau*. Deltares Report 1207384 to Wetlands International, CLUA and Norad.

- Hoyt, A. M., Chaussard, E., Seppalainen, S. S., & Harvey, C. F. (2020). Widespread subsidence and carbon emissions across Southeast Asian peatlands. *Nature Geoscience*, 13(6), 435–440. <https://doi.org/10.1038/s41561-020-0575-4>
- Husnain, H., Wigena, I. G. P., Dariah, A., Marwanto, S., Setyanto, P., & Agus, F. (2014). CO2 emissions from tropical drained peat in Sumatra, Indonesia. *Mitigation and Adaptation Strategies for Global Change*, 19(6), 845–862. <https://doi.org/10.1007/s11027-014-9550-y>
- Ichsan, N., Vernimmen, R., Hooijer, A., & Applegate, G. (2012). *KECP Hydrology and Peat Monitoring Methodology*. IAFCP.
- Jauhiainen, J., Hooijer, A., & Page, S. E. (2012). Carbon dioxide emissions from an *Acacia* plantation on peatland in Sumatra, Indonesia. *Biogeosciences*, 9(2), 617–630. <https://doi.org/10.5194/bg-9-617-2012>
- Jaya, A., Murdiyarso, D., Sasmito, S. D., & Rumbang, N. (2016, August 15). *Surface elevation changes of tropical peatland under different land covers: A Preliminary account following 2015 fires in Central Kalimantan, Indonesia*. 2016 International Peat Society Congress, Serawak
- Jolivet, R., Grandin, R., Lasserre, C., Doin, M.-P., & Peltzer, G. (2011). Systematic InSAR tropospheric phase delay corrections from global meteorological reanalysis data. *Geophysical Research Letters*, 38(17), n/a-n/a. <https://doi.org/10.1029/2011GL048757>
- Juniyanti, L., Prasetyo, L. B., Aprianto, D. P., Purnomo, H., & Kartodihardjo, H. (2020). Perubahan Penggunaan dan Tutupan Lahan, Serta Faktor Penyebabnya di Pulau Bengkalis, Provinsi Riau (periode 1990-2019). *Jurnal Pengelolaan Sumberdaya Alam*

- Dan Lingkungan (Journal of Natural Resources and Environmental Management)*, 10(3), 419–435. <https://doi.org/10.29244/jpsl.10.3.419-435>
- Kadavi, P. R., & Lee, C.-W. (2018). Land cover classification analysis of volcanic island in Aleutian Arc using an artificial neural network (ANN) and a support vector machine (SVM) from Landsat imagery. *Geosciences Journal*, 22(4), 653–665. <https://doi.org/10.1007/s12303-018-0023-2>
- Karasiak, N. (2019). *Lennepkade/dzetsaka: Dzetsaka v3.5.1 (v3.5.1)* [Computer software]. <https://doi.org/10.5281/ZENODO.2552284>
- Key, C. H., & Benson, N. C. (2005). Landscape assessment. Ground measure of severity, the Composite Burn Index; and remote sensing of severity, the Normalized Burn Ratio. In D. C. Lutes, R. E. Keane, J. F. Caratti, C. H. Key, N. C. Benson, & L. J. Gangi (Eds.), *FIREMON: Fire Effects Monitoring and Inventory System*. USDA Forest Service, Rocky Mountains Research Station General Technical Report.
- Khakim, M. Y. N., Bama, A. A., Yustian, L., Poerwono, P., Tsuji, T., & Matsuoka, T. (2020). Peatland subsidence and vegetation cover degradation as impacts of the 2015 El niño event revealed by Sentinel-1A SAR data. *International Journal of Applied Earth Observation and Geoinformation*, 84, 101953. <https://doi.org/10.1016/j.jag.2019.101953>
- Lewis, K., Rumpang, E., Kho, L. K., McCalmont, J., Teh, Y. A., Gallego-Sala, A., & Hill, T. C. (2020). An assessment of oil palm plantation aboveground biomass stocks on tropical peat using destructive and non-destructive methods. *Scientific Reports*, 10(1), 2230. <https://doi.org/10.1038/s41598-020-58982-9>

- Liu, P., Choo, K.-K. R., Wang, L., & Huang, F. (2017). SVM or deep learning? A comparative study on remote sensing image classification. *Soft Computing*, *21*(23), 7053–7065.  
<https://doi.org/10.1007/s00500-016-2247-2>
- Llano, X. C. (2019). *AcATaMa—QGIS plugin for Accuracy Assessment of Thematic Maps, version 19.11.21*. <https://plugins.qgis.org/plugins/AcATaMa/>
- Loisel, J., Gallego-Sala, A. V., Amesbury, M. J., Magnan, G., Anshari, G., Beilman, D. W., Benavides, J. C., Blewett, J., Camill, P., Charman, D. J., Chaychai, S., Hedgpeth, A., Kleinen, T., Korhola, A., Large, D., Mansilla, C. A., Miller, J., van Bellen, S., West, J. B., ... Wu, J. (2021). Expert assessment of future vulnerability of the global peatland carbon sink. *Nature Climate Change*, *11*(1), 70–77. <https://doi.org/10.1038/s41558-020-00944-0>
- Louppe, G., Wehenkel, L., Sutera, A., & Geurts, P. (2013). Understanding variable importances in forests of randomized trees. *Advances in Neural Information Processing Systems*, 431–439.
- Mansaray, L. R., Wang, F., Huang, F., Yang, L., & Kanu, A. S. (2020). Accuracies of support vector machine and random forest in rice mapping with Sentinel-1A, Landsat-8 and Sentinel-2A datasets. *Geocarto International*, *35*(10), 1088–1108.  
<https://doi.org/10.1080/10106049.2019.1568586>
- Marshall, C., Large, D. J., Athab, A., Evers, S. L., Sowter, A., Marsh, S., & Sjögersten, S. (2018). Monitoring tropical peat related settlement using ISBAS InSAR, Kuala Lumpur International Airport (KLIA). *Engineering Geology*, *244*, 57–65.  
<https://doi.org/10.1016/j.enggeo.2018.07.015>
- Masek, J. G., Vermote, E. F., Saleous, N. E., Wolfe, R., Hall, F. G., Huemmrich, K. F., Gao, F., Kutler, J., & Lim, T.-K. (2006). A Landsat Surface Reflectance Dataset for North

- America, 1990–2000. *IEEE Geoscience and Remote Sensing Letters*, 3(1), 68–72.  
<https://doi.org/10.1109/LGRS.2005.857030>
- McCarthy, J. F. (2010). Processes of inclusion and adverse incorporation: Oil palm and agrarian change in Sumatra, Indonesia. *The Journal of Peasant Studies*, 37(4), 821–850.  
<https://doi.org/10.1080/03066150.2010.512460>
- Miettinen, J., Hooijer, A., Vernimmen, R., Liew, S. C., & Page, S. E. (2017). From carbon sink to carbon source: Extensive peat oxidation in insular Southeast Asia since 1990. *Environmental Research Letters*, 12(2), 024014. <https://doi.org/10.1088/1748-9326/aa5b6f>
- Miettinen, J., Shi, C., & Liew, S. C. (2016). Land cover distribution in the peatlands of Peninsular Malaysia, Sumatra and Borneo in 2015 with changes since 1990. *Global Ecology and Conservation*, 6, 67–78. <https://doi.org/10.1016/j.gecco.2016.02.004>
- Minh, D. H. T., Hanssen, R., & Rocca, F. (2020). Radar Interferometry: 20 Years of Development in Time Series Techniques and Future Perspectives. *Remote Sensing*, 12(9), 1364. <https://doi.org/10.3390/rs12091364>
- Olofsson, P., Foody, G. M., Herold, M., Stehman, S. V., Woodcock, C. E., & Wulder, M. A. (2014). Good practices for estimating area and assessing accuracy of land change. *Remote Sensing of Environment*, 148, 42–57. <https://doi.org/10.1016/j.rse.2014.02.015>
- Osaki, M., Nursyamsi, D., Noor, M., Wahyunto, & Segah, H. (2016). Peatland in Indonesia. In M. Osaki & N. Tsuji (Eds.), *Tropical Peatland Ecosystems* (pp. 49–58). Springer Japan.  
[https://doi.org/10.1007/978-4-431-55681-7\\_3](https://doi.org/10.1007/978-4-431-55681-7_3)

- Osmanoğlu, B., Sunar, F., Wdowinski, S., & Cabral-Cano, E. (2016). Time series analysis of InSAR data: Methods and trends. *ISPRS Journal of Photogrammetry and Remote Sensing*, *115*, 90–102. <https://doi.org/10.1016/j.isprsjprs.2015.10.003>
- Othman, H., Darus, F. M., & Mohammed, A. T. (2009). Experiences in peat development for oil palm planting in the MPOB Research Station at Sessang, Sarawak. *Oil Palm Bulletin*, *58*, 1–9.
- Page, S. E., Rieley, J. O., & Banks, C. J. (2011). Global and regional importance of the tropical peatland carbon pool. *Global Change Biology*, *17*(2), 798–818. <https://doi.org/10.1111/j.1365-2486.2010.02279.x>
- Park, S.-W., Jung, S.-W., & Hong, S.-H. (2020). ALOS-2 Stripmap-ScanSAR 위상간섭기법에서의 스펙트럼 분석 평가. *대한원격탐사학회지*, *36*(2\_2), 351–363. <https://doi.org/10.7780/KJRS.2020.36.2.2.10>
- Pepe, A., & Calò, F. (2017). A Review of Interferometric Synthetic Aperture RADAR (InSAR) Multi-Track Approaches for the Retrieval of Earth's Surface Displacements. *Applied Sciences*, *7*(12), 1264. <https://doi.org/10.3390/app7121264>
- Prastyaningsih, S. R., Harjwinoto, S., Agus, C., & Musyafa. (2019). Development Paludiculture on Tropical Peatland for Productive and Sustainable Ecosystem in Riau. *IOP Conference Series: Earth and Environmental Science*, *256*, 012048. <https://doi.org/10.1088/1755-1315/256/1/012048>
- Purnomo, E. P., Ramdani, R., Agustiyara, Tomaro, Q. P. V., & Samidjo, G. S. (2019). Land ownership transformation before and after forest fires in Indonesian palm oil plantation areas. *Journal of Land Use Science*, *14*(1), 37–51. <https://doi.org/10.1080/1747423X.2019.1614686>

- Reeve, A. S., Glaser, P. H., & Rosenberry, D. O. (2013). Seasonal changes in peatland surface elevation recorded at GPS stations in the Red Lake Peatlands, northern Minnesota, USA. *Journal of Geophysical Research: Biogeosciences*, *118*(4), 1616–1626.  
<https://doi.org/10.1002/2013JG002404>
- Rijal, S. (2019). Typology of Deforestation in Riau Province. *IOP Conference Series: Earth and Environmental Science*, *270*, 012040. <https://doi.org/10.1088/1755-1315/270/1/012040>
- Rosen, P. A., Gurrola, E., Sacco, G. F., & Zebker, H. (2012). *The InSAR scientific computing environment*. 730–733.
- Rouse, J. W., Haas, R. H., Schell, J. A., & Deering, D. W. (1974). Monitoring vegetation systems in the Great Plains with ERTS. *NASA Special Publication*, *351*(1974), 309.
- Rudiyanto, Minasny, B., Setiawan, B. I., Saptomo, S. K., & McBratney, A. B. (2018). Open digital mapping as a cost-effective method for mapping peat thickness and assessing the carbon stock of tropical peatlands. *Geoderma*, *313*, 25–40.  
<https://doi.org/10.1016/j.geoderma.2017.10.018>
- Sowter, A., Bateson, L., Strange, P., Ambrose, K., & Syafiudin, Moh. F. (2013). DInSAR estimation of land motion using intermittent coherence with application to the South Derbyshire and Leicestershire coalfields. *Remote Sensing Letters*, *4*(10), 979–987.  
<https://doi.org/10.1080/2150704X.2013.823673>
- Stockamp, J. (2018). *Establishing wide-scale mapping of vertical land motion with advanced DInSAR time series analysis in Scotland* [PhD thesis]. University of Glasgow.
- Supardi, Subekty, A. D., & Neuzil, S. G. (1993). General geology and peat resources of the Siak Kanan and Bengkalis Island peat deposits, Sumatra, Indonesia. In *Geological Society of*

- America Special Papers* (Vol. 286, pp. 45–62). Geological Society of America.  
<https://doi.org/10.1130/SPE286-p45>
- Tan, Z. D., Lupascu, M., & Wijedasa, L. S. (2021). Paludiculture as a sustainable land use alternative for tropical peatlands: A review. *Science of The Total Environment*, 753, 142111. <https://doi.org/10.1016/j.scitotenv.2020.142111>
- Umarhadi, D. A., Avtar, R., Widyatmanti, W., Johnson, B. A., Yunus, A. P., Khedher, K. M., & Singh, G. (2021). Use of multi - frequency (C - band and L - band) SAR data to monitor peat subsidence based on time - series SBAS InSAR technique. *Land Degradation & Development*, ldr.4061. <https://doi.org/10.1002/ldr.4061>
- van der Linden, S., Rabe, A., Held, M., Jakimow, B., Leitão, P., Okujeni, A., Schwieder, M., Suess, S., & Hostert, P. (2015). The EnMAP-Box—A Toolbox and Application Programming Interface for EnMAP Data Processing. *Remote Sensing*, 7(9), 11249–11266. <https://doi.org/10.3390/rs70911249>
- Vapnik, V. N. (2000). *The nature of statistical learning theory* (2nd ed). Springer.
- Webb, E. L., Friess, D. A., Krauss, K. W., Cahoon, D. R., Guntenspergen, G. R., & Phelps, J. (2013). A global standard for monitoring coastal wetland vulnerability to accelerated sea-level rise. *Nature Climate Change*, 3(5), 458–465. <https://doi.org/10.1038/nclimate1756>
- Wei, M., & Sandwell, D. T. (2010). Decorrelation of L-Band and C-Band Interferometry Over Vegetated Areas in California. *IEEE Transactions on Geoscience and Remote Sensing*, 48(7), 2942–2952. <https://doi.org/10.1109/TGRS.2010.2043442>
- Wösten, J. H. M., Ismail, A. B., & van Wijk, A. L. M. (1997). Peat subsidence and its practical implications: A case study in Malaysia. *Geoderma*, 78(1–2), 25–36.  
[https://doi.org/10.1016/S0016-7061\(97\)00013-X](https://doi.org/10.1016/S0016-7061(97)00013-X)

- Xue, F., Lv, X., Dou, F., & Yun, Y. (2020). A Review of Time-Series Interferometric SAR Techniques: A Tutorial for Surface Deformation Analysis. *IEEE Geoscience and Remote Sensing Magazine*, 8(1), 22–42. <https://doi.org/10.1109/MGRS.2019.2956165>
- Yamamoto, K., Basir, N., Sutikno, S., Kanno, A., Kagawa, H., Suzuki, M., Akamatsu, Y., & Koyama, A. (2019). Tropical peat debris storage in the tidal flat in northern part of the Bengkalis island, Indonesia. *MATEC Web of Conferences*, 276, 06002. <https://doi.org/10.1051/mateconf/201927606002>
- Yu, Z., Loisel, J., Brosseau, D. P., Beilman, D. W., & Hunt, S. J. (2010). Global peatland dynamics since the Last Glacial Maximum. *Geophysical Research Letters*, 37(13). <https://doi.org/10.1029/2010GL043584>
- Yunjun, Z., Fattahi, H., & Amelung, F. (2019). Small baseline InSAR time series analysis: Unwrapping error correction and noise reduction. *Computers & Geosciences*, 133, 104331. <https://doi.org/10.1016/j.cageo.2019.104331>
- Zhou, Z., Li, Z., Waldron, S., & Taraka, A. (2019). InSAR Time Series Analysis of L-Band Data for Understanding Tropical Peatland Degradation and Restoration. *Remote Sensing*, 11(21), 2592. <https://doi.org/10.3390/rs11212592>

### Figure Captions

**Figure 1:** Conceptual diagram illustrating the process of peat subsidence with the influence of drainage period and LULC change.

**Figure 2:** Location of the study area (part of Bengkalis Island) with Landsat 8 image (composite of 654) acquired on 11/02/2019. Peat area is delineated referring to Supardi et al., (1993). The northern tip of the island is a coastal erosion area, which is excluded in our analysis. SIPALAGA

(Peatland Water Monitoring System) data were provided by the Peatland Restoration Agency of Indonesia.

**Figure 3:** Flowchart describing the methodology of this study.

**Figure 4:** Flowchart of SBAS InSAR processing.

**Figure 5:** (a) Baseline plot showing the network of interferograms with the average spatial coherence value, and (b) RMS value plot of residual phase showing the elimination of displacement image higher than the threshold (three times the median value).

**Figure 6:** Vertical displacement with the reference of the first date (13/02/2016). A black dot in the first image indicates the location of the reference point.

**Figure 7:** Vertical velocity calculated within a period of (a) 13/02/2016 to 24/08/2019 and (b) 27/01/2018 to 24/08/2019 with (c and d) the scatterplots in a relationship with GWL based annual subsidence, respectively.

**Figure 8:** (a) Land use/land cover (LULC) maps for 1972, 1988, 1998, 2010, 2015, and 2019; (b) drainage period derived from the LULC maps. The northern tip of Area I is masked due to coastal erosion, as well as mangroves and water bodies considered as non-peat areas.

**Figure 9:** (a) Mean vertical velocity (cm/year) of recent LULC (2019) categorized based on general drainage periods (dashed lines) and more specific drainage periods after 1972 (solid bars). (b) Results of Mann-Whitney U-test showing whether subsidence rate significantly decelerated over time (asterisk symbol shows that the decrease is significant).

**Figure 10:** (a) Distance from peat edge and (b) elevation data with scatterplots (c and d) showing the relationship with vertical velocity.

**Figure 11:** Vertical velocity derived from (a) Random Forest regression (ntrees = 1000); (b) Scatterplot; and (c) profile lines for comparison between the RF model and SBAS InSAR.

Journal Pre-proof

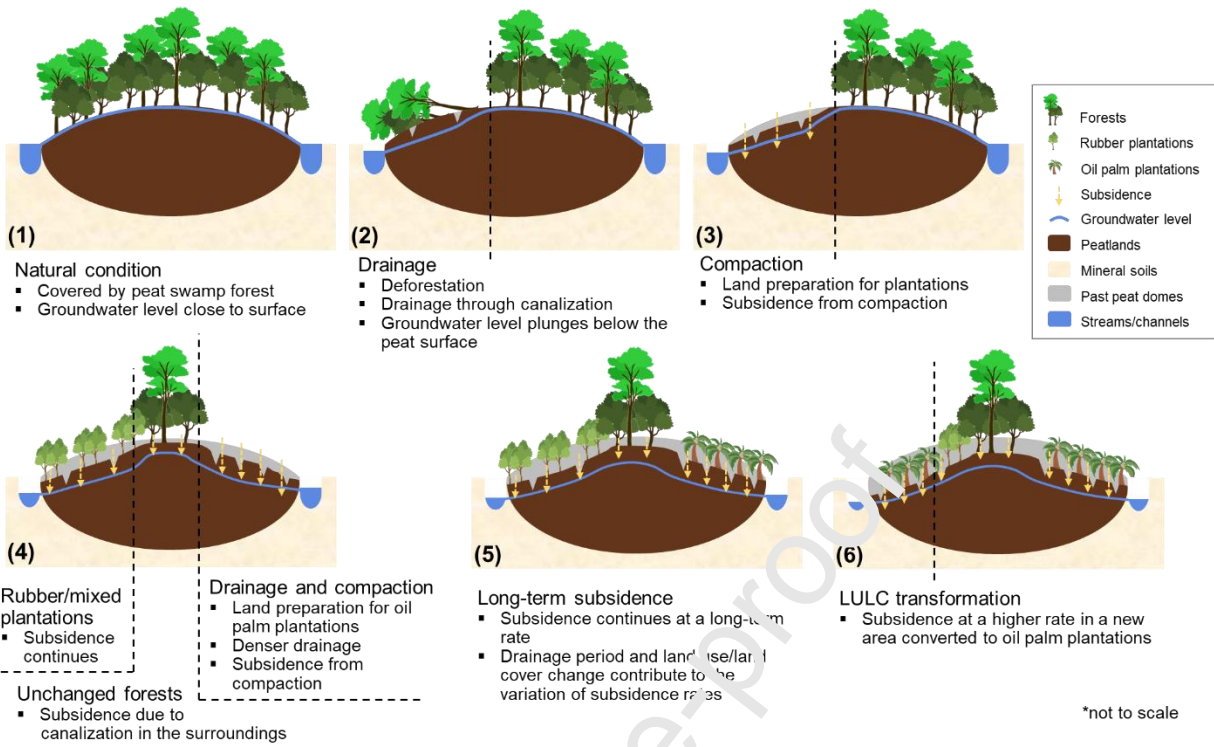


**Figure 1:** Conceptual diagram illustrating the process of peat subsidence with the influence of drainage period and LULC change.

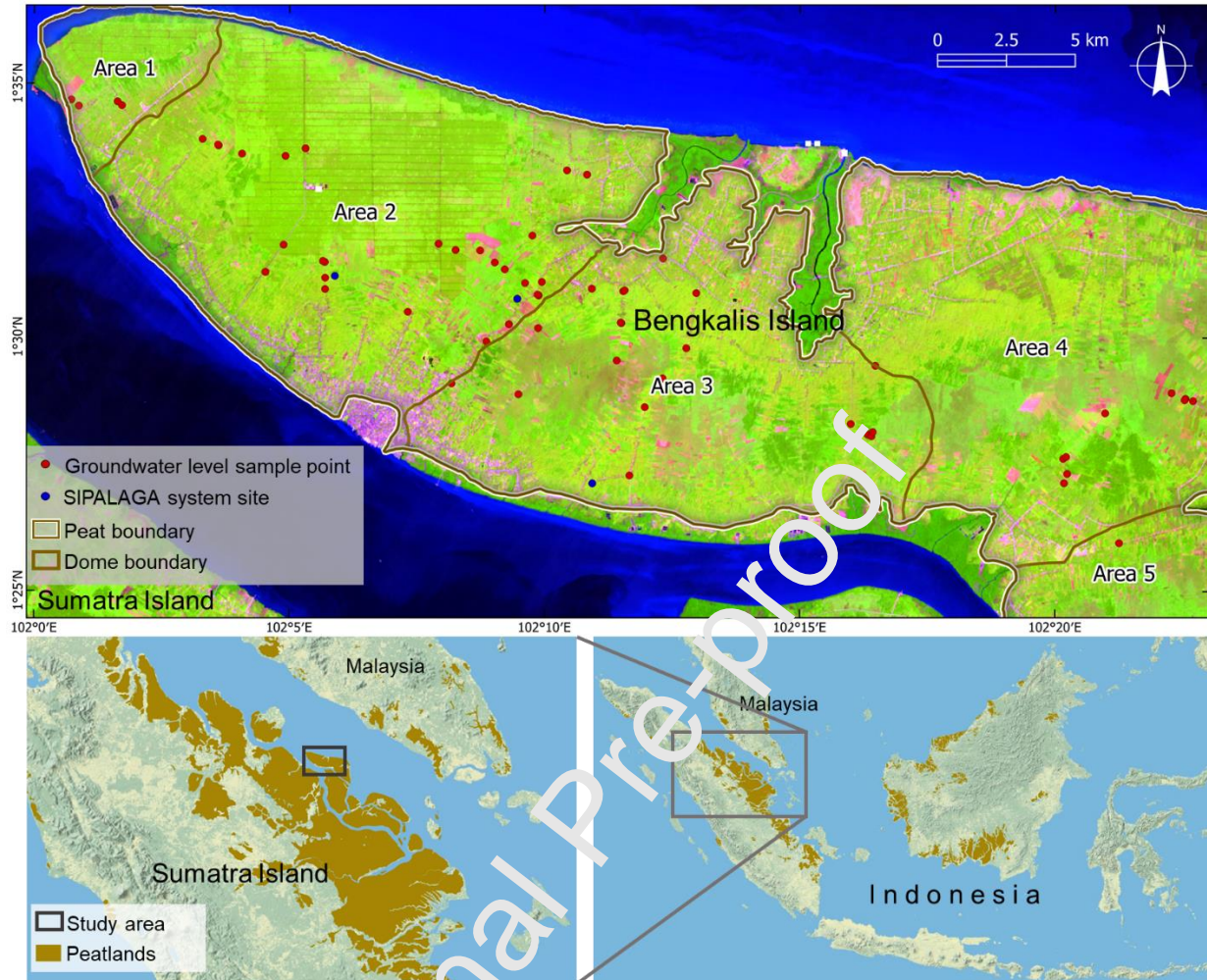


**Figure 2:** Location of the study area (part of Bengkalis Island) with Landsat 8 image (composite of 654) acquired on 11/02/2019. Peat area is delineated referring to Supardi et al., (1993). The northern tip of the island is a coastal erosion area, which is excluded in our analysis. SIPALAGA (Peatland Water Monitoring System) data were provided by the Peatland Restoration Agency of Indonesia.

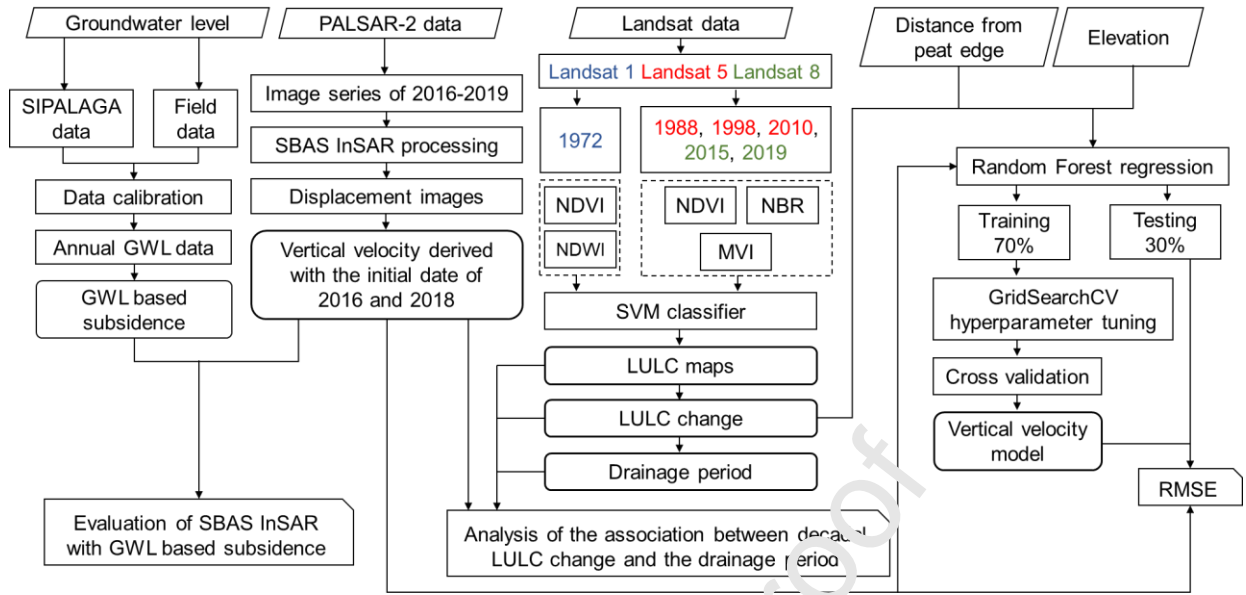


Figure 3: Flowchart describing the methodology of this study.

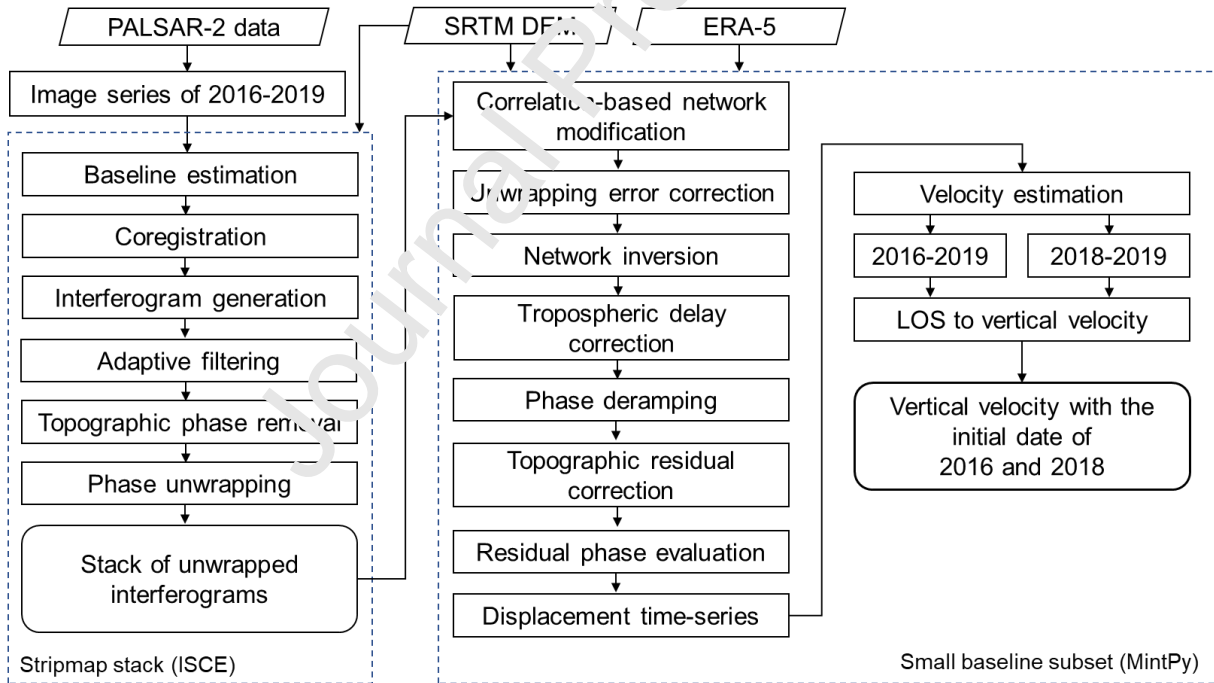
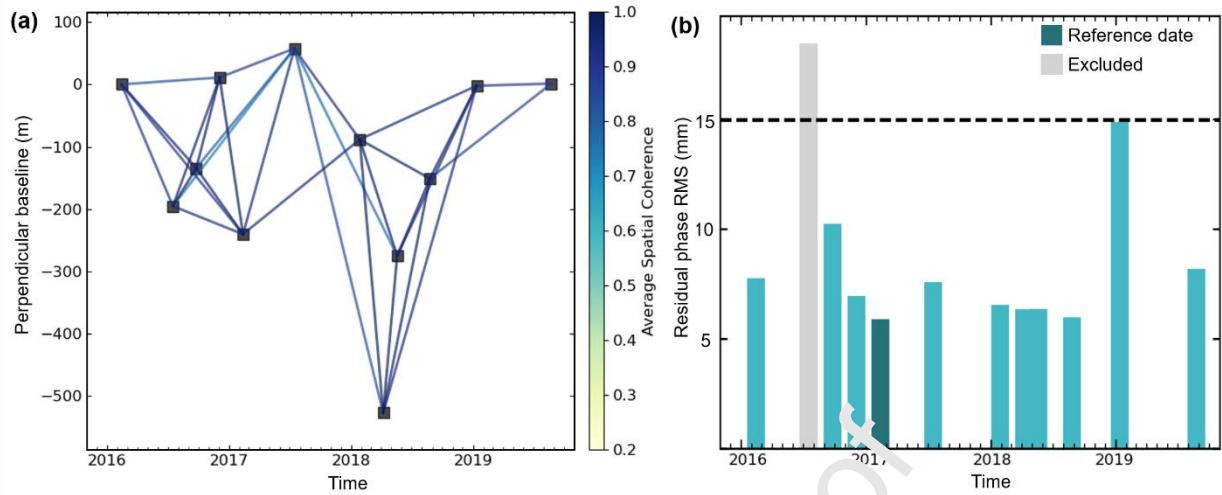
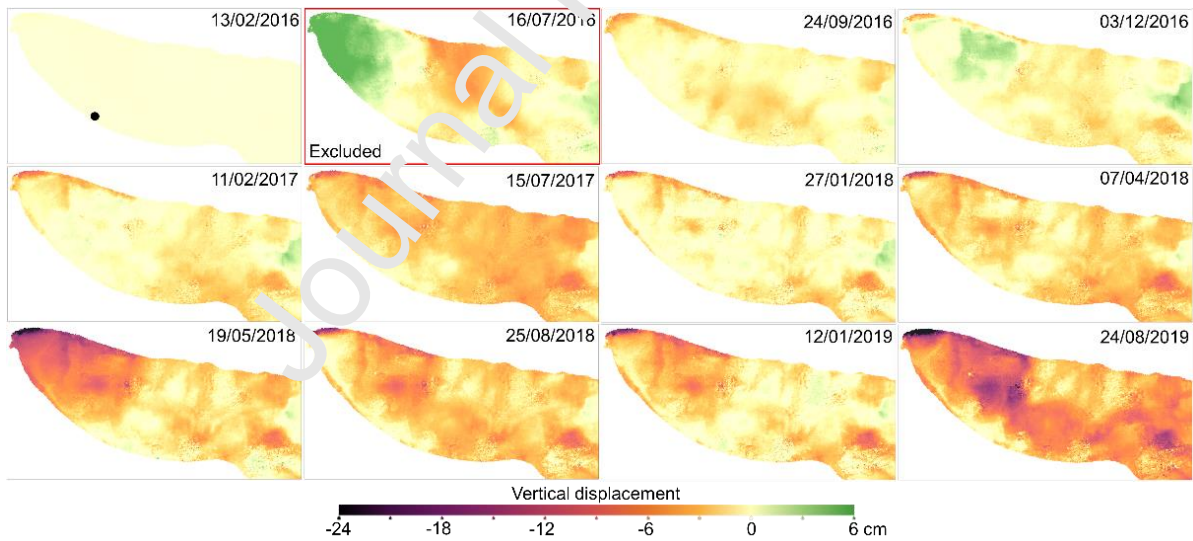


Figure 4: Flowchart of SBAS InSAR processing.



**Figure 5:** (a) Baseline plot showing the network of interferograms with the average spatial coherence value, and (b) RMS value plot of residual phase showing the elimination of displacement image higher than the threshold (three times the median value).



**Figure 6:** Vertical displacement with the reference of the first date (13/02/2016). A black dot in the first image indicates the location of the reference point.

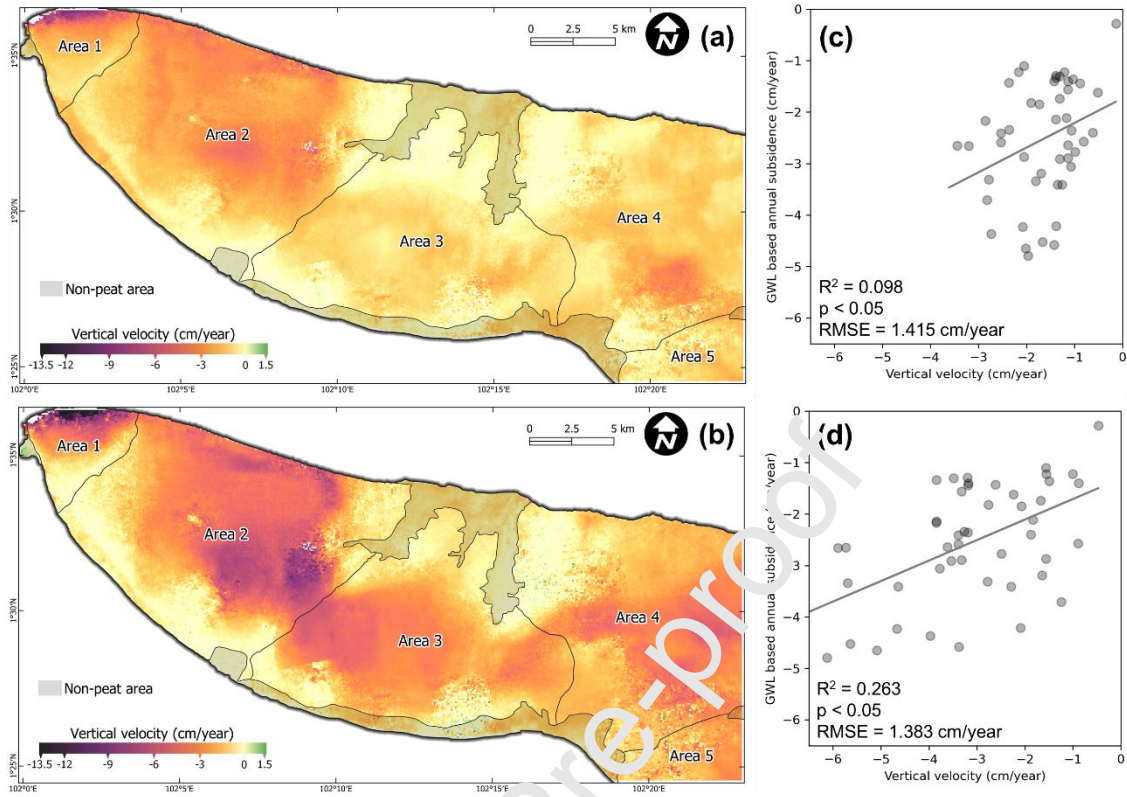


**Figure 7:** Vertical velocity calculated within a period of (a) 13/02/2016 to 24/08/2019 and (b) 27/01/2018 to 24/08/2019 with (c and d) the scatterplots in a relationship with GWL based annual subsidence, respectively.

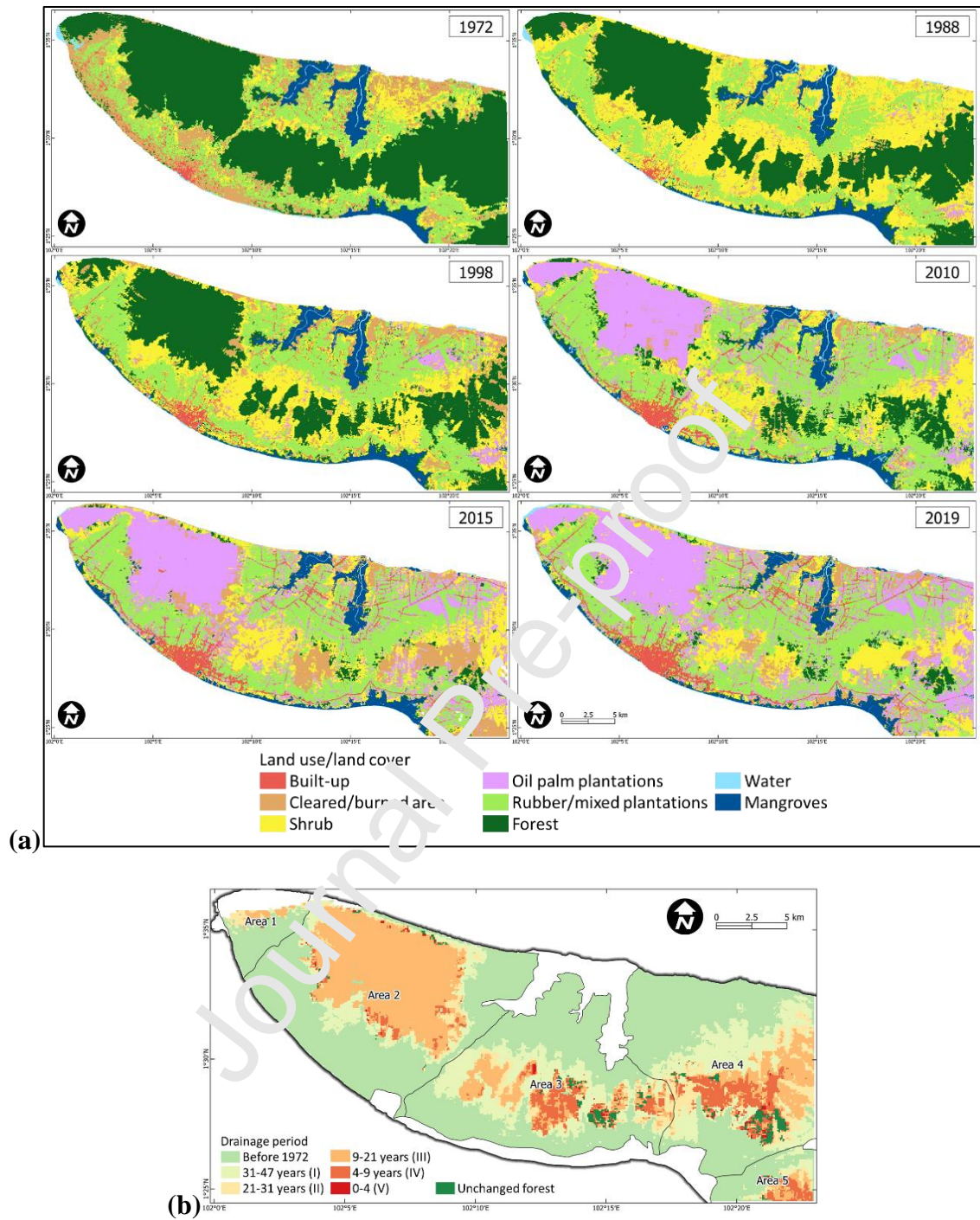


**Figure 8:** (a) Land use/land cover (LULC) maps for 1972, 1988, 1998, 2010, 2015, and 2019; (b) drainage period derived from the LULC maps. The northern tip of Area I is masked due to coastal erosion, as well as mangroves and water bodies considered as non-peat areas.

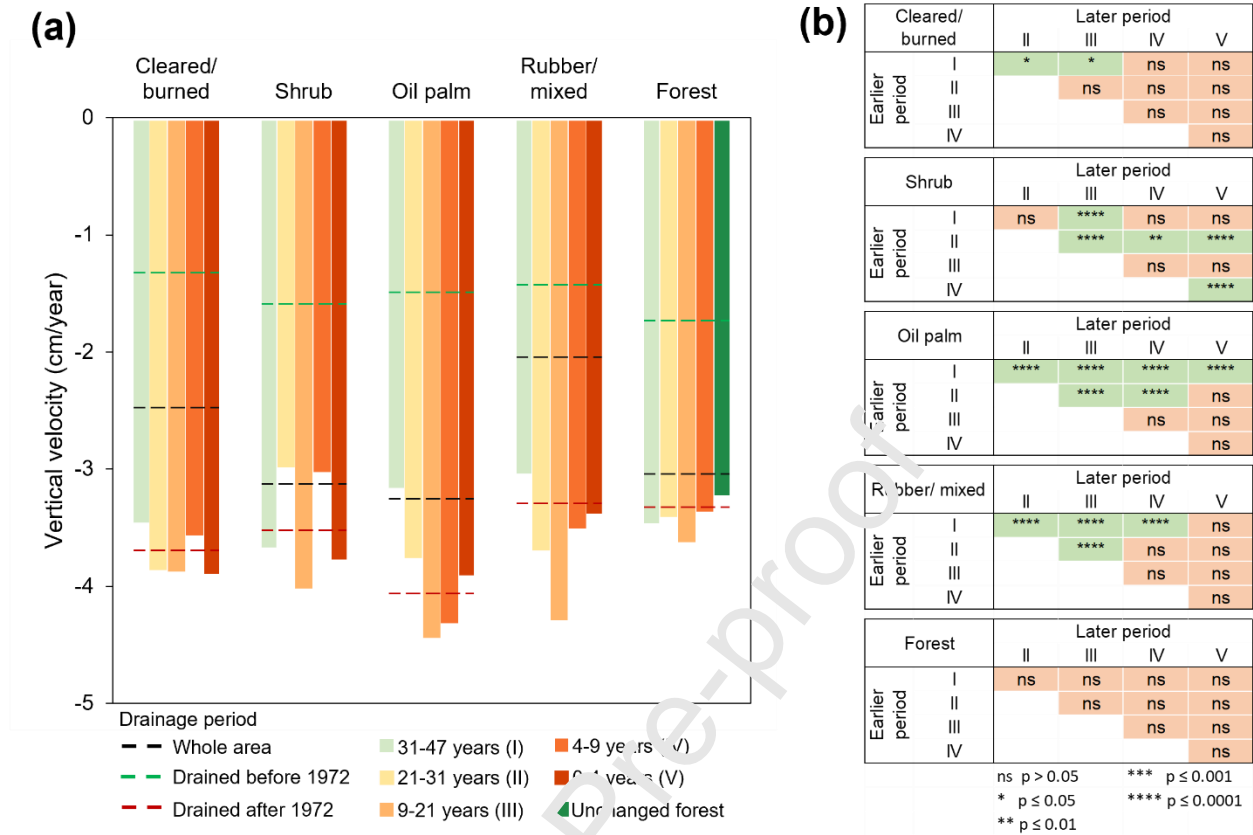


**Figure 9:** (a) Mean vertical velocity (cm/year) of recent LULC (2019) categorized based on general drainage periods (dashed lines) and more specific drainage periods after 1972 (solid bars). (b) Results of Mann-Whitney U-test showing whether subsidence rate significantly decelerated over time (asterisk symbol shows that the decrease is significant).

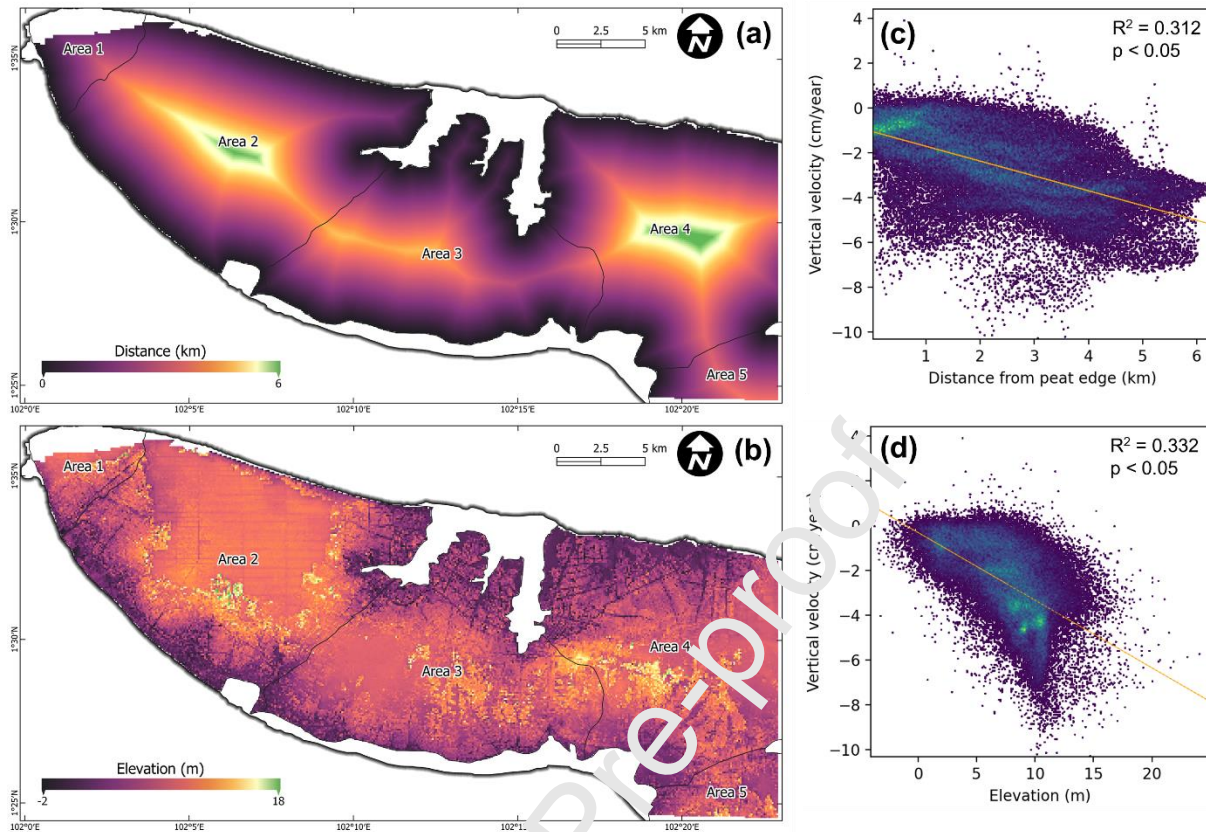


**Figure 10:** (a) Distance from peat edge and (b) elevation data with scatterplots (c and d) showing the relationship with vertical velocity.

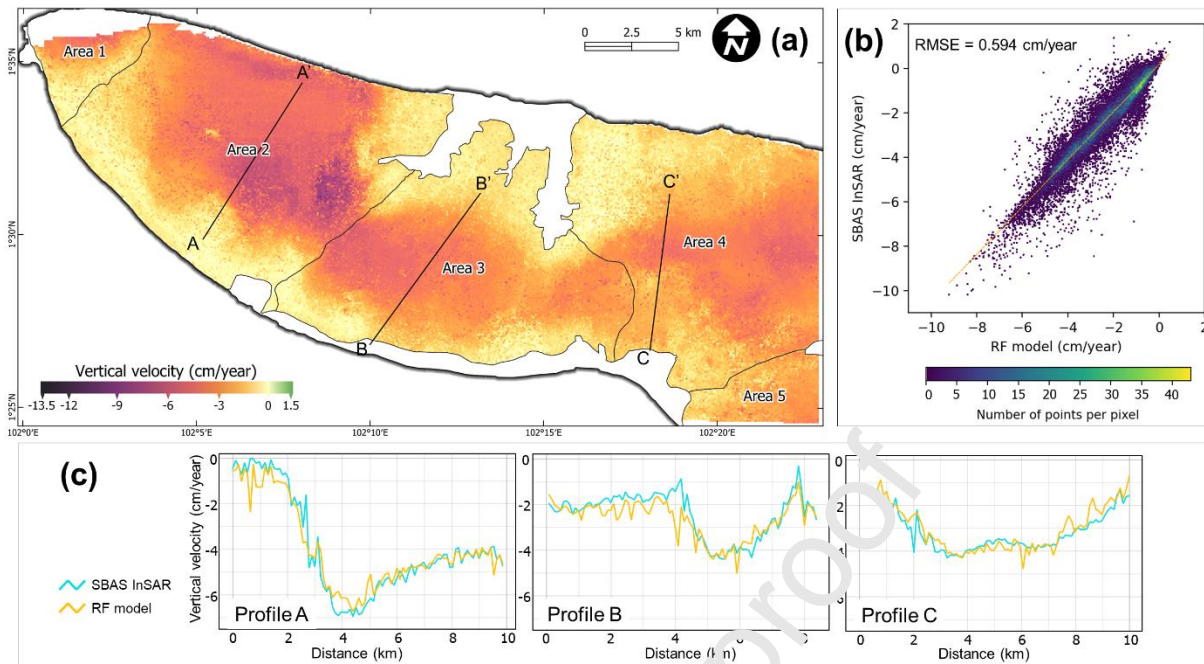


**Figure 11:** Vertical velocity derived from (a) Random Forest regression (ntrees = 1000); (b) Scatterplot; and (c) profile lines for comparison between the RF model and SBAS InSAR.

**Table 1:** List of PALSAR-2 SAR data.

Date	Time interval (days)	Perpendicular baseline (m)
13/02/2016	-	-
16/07/2016	154	-195.3
24/09/2016	70	-134.2
03/12/2016	70	11.1
11/02/2017	70	-240.4
15/07/2017	154	57.6
27/01/2018	196	-88.4
07/04/2018	70	-527.0
19/05/2018	42	-275.2
25/08/2018	98	-151.1
12/01/2019	140	-2.2
24/08/2019	224	1.2

**Table 2:** List of Landsat images.

Image acquisition	Landsat sensor	Pixel size	Bands used
05/10/1972	Landsat 1	60 m	Green, Red, Near Infrared (NIR) 1, NIR 2
22/12/1988	Landsat 5	30 m	Blue, Green, Red, NIR,
27/07/1998	Landsat 5	30 m	Shortwave Infrared
02/02/2010	Landsat 5	30 m	(SWIR) 1, SWIR 2
15/01/2015	Landsat 8	30 m	Blue, Green, Red, NIR,

11/02/2019

Landsat 8

30 m

SWIR 1, SWIR 2

**Table 3:** LULC area in percentage, color-coded from blue (low percentage) to red (high percentage).

LULC class	Area in percent (%)					
	1972	1988	1998	2010	2015	2019
Built-up	1.94	0.68	2.19	3.28	4.66	5.37
Cleared/burned area	13.85	4.36	8.34	4.43	11.41	6.27
Shrub	8.66	34.33	26.15	18.59	16.76	14.27
Oil palm plantations	0.00	0.61	2.35	20.56	27.85	31.12
Rubber/mixed plantations	21.69	19.53	25.40	36.95	30.78	33.93
Forest	48.43	34.23	29.55	9.68	2.75	3.33
Water	0.66	1.01	0.63	1.07	0.57	1.06
Mangroves	4.77	5.26	5.40	5.43	5.22	4.65
Accuracy (%)	81.60	83.17	85.55	83.20	83.76	80.04
Weighted F1 score (%)	81.95	81.90	85.22	82.87	83.78	79.45

**Table 4.** LULC change matrix with mean vertical velocity values (cm/year), color-coded from blue (high value) to red (low value). Change matrices with multiple years in the heading indicate no further LULC changes after the first mentioned year. Only values with more than 10 pixels are included in the table.

		LULC 2019				
		Cleared/ burned	Shrub	Oil palm	Rubber/ mixed	Forest
LULC	Cleared/burned	-3.512	-3.043	-4.474	-4.320	-4.368
2015	Shrub	-4.018	-3.981	-3.775	-3.686	-3.523

	Oil palm	-3.283	-3.269	-4.102	-3.527	-3.634
	Rubber/mixed	-4.074	-3.730	-3.263	-2.873	-3.411
	Forest	-3.792	-3.876	-3.664	-3.268	-3.196
LULC 2015 and 2019						
LULC 2010	Cleared/burned	-3.336	-3.935	-4.987	-2.983	
	Shrub	-3.469	-3.979	-4.120	-3.417	-4.084
	Oil palm	-3.472	-4.014	-4.129	-2.891	
	Rubber/mixed	-3.775	-4.070	-3.238	-2.735	-3.365
	Forest	-3.474	-3.561	-3.716	-2.933	-3.174
LULC 2010, 2015, and 2019						
LULC 1998	Cleared/burned		-4.223	-3.120	-2.890	
	Shrub	-3.498	-3.453	-3.108	-2.860	-3.215
	Oil palm			-2.335	-2.317	
	Rubber/mixed		-3.184		-2.518	
	Forest	-3.551	-4.288	-4.347	-2.990	-3.178
LULC 1998, 2010, 2015, and 2019						
LULC 1988	Cleared/burned		-3.101	-2.292	-2.841	
	Shrub		-3.915	-2.316	-2.537	-2.401
	Oil palm			-2.465		
	Rubber/mixed				-2.271	
	Forest		-2.912		-2.633	-3.224

### **Credit Author Statements**

Deha Agus Umarhadi is responsible for data collection, data processing, overall investigation, and writing;

Ram Avtar and Wirastuti Widyatmanti are responsible for supervision, resources and conceptualization;

Pankaj Kumar, Ali P. Yunus, Khaled Mohamed Khedher, Mamoru Ishikawa and Ali Kharrazi are responsible for analysis and reviewing the manuscript.

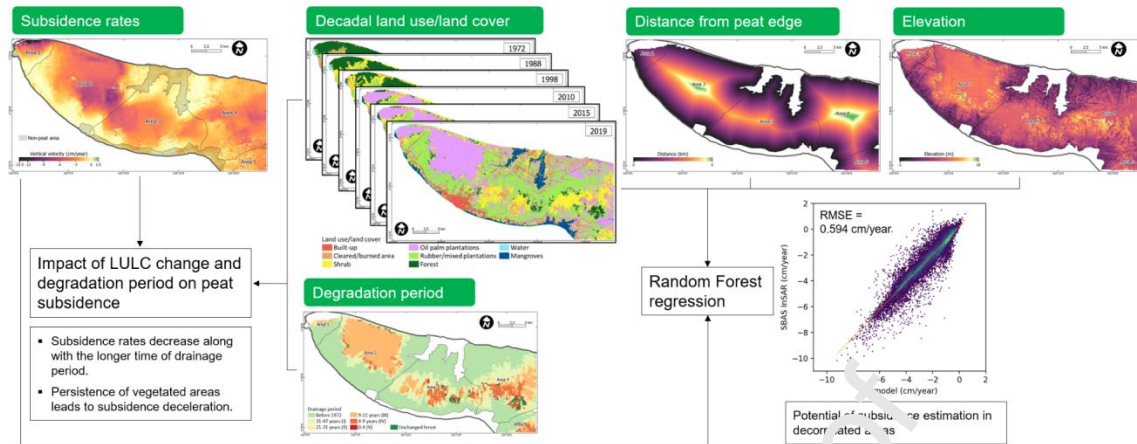
Journal Pre-proof

**Declaration of interests**

The authors declare that they have no known competing financial interests or personal relationships that could have appeared to influence the work reported in this paper.

Journal Pre-proof

## Graphical Abstract



### Highlights

- SBAS InSAR reveals subsidence in degraded peatlands in a tropical Island.
- Subsidence rate decreases along with the longer time of drainage period.
- Persistence of vegetated areas leads to subsidence deceleration.

Journal Pre-proof